Sedimentary Geology 496 (2026) 107055

Contents lists available at ScienceDirect

Sedimentary Geology

journal homepage: www.elsevier.com/locate/sedgeo

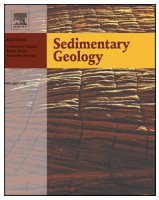

Deciphering the Eocene carbonate platforms of the Bekrit-Timahdite sector (Middle Atlas, Morocco): The gateway to the Atlantic Domain

Manuel Martín-Martín [a,*], Josep Tosquella [b], Crina Miclăuș [c], Ali Maaté [d], José Enrique Tent-Manclús [a], Soufian Maaté [d], Eric Monteil [e], Francisco Serrano [f], José Antonio Martín-Pérez [a]

[a] Departamento de Ciencias de la Tierra y Medio Ambiente, University of Alicante, Alicante, Spain
[b] Departamento de Ciencias de la Tierra, University of Huelva, Huelva, Spain
[c] Departmentul de Geologie, "Alexandru Ioan Cuza" University, Iași, Romania
[d] Laboratoire de Géologie de l'Environnement et Ressources Naturelles, FS, Abdelmalek Essaâdi University, Tetouan, Morocco
[e] TimeMatters España, Alicante, Spain
[f] Departamento de Ecología y Geología, University of Málaga, Málaga, Spain

ARTICLE INFO

Editor: Dr. Catherine Chagué

Keywords:
Eocene carbonate platforms
Oyster reefs
Paleoenvironmental evolution
Atlantic Domain
Eo-Alpine tectonic phase

ABSTRACT

This study identifies thirteen sedimentary facies (F1 to F13) across five stratigraphic sections, representing shallow marine carbonate platform environments. These are characterized by lithology, sedimentary structures, and macrofossil content including oysters, gastropods, echinoids, algae, fish remains, and bryozoans. A total absence of larger benthic foraminifera (LBF) and zooxanthellate corals (z-corals) has been noticed. Biostratigraphic analysis dated the basement as Maastrichtian (non terminal) and the Paleogene succession as Lutetian. Eight carbonate platform microfacies (Mf1 to Mf8) were defined, covering both inner ramp (tidal flat, lagoon, shoal, and oyster-rich reef bioherm) and mid ramp (reef slope and open marine) environments. The Eocene fossil assemblage indicates the presence of heterotrophic communities thriving in meso- to eutrophic waters, indicative of a tropical, heterozoan carbonate factory dominated by bryozoans and mollusks. Subsidence patterns varied significantly: Logs 4 and 5 (Folded Middle Atlas Block) recorded higher subsidence rates, while Logs 1 to 3 (Tabular Middle Atlas Block) show lower rates. Succession is organized into low-frequency (3rd-order) predominantly transgressive sequences, typically punctuated by rapid regressions and transgressions. These depositional rhythms are interpreted as responses to regional tectonic pulses associated with the Eo-Alpine phase. Regional correlations reveal a striking contrast: while coeval Neo-Tethyan platforms, from Spain to Italy, are characterized by homogeneity and abundant LBF and z-corals, the study area and the Algerian Saharan Domain, lack these taxa, instead featuring sediments rich in phosphates, oysters, and fish remains. This distinctive facies association (heterozoan dominated) reflects nutrient-rich upwelling zones similar to those in the Atlantic. It is proposed that further exploration of a potential narrow corridor, which served as hinterland to the Atlas-Mesetas System during the Paleocene-Eocene period and was influenced by tectonic controls from basement folding, could elucidate the origin of these Atlantic-type deposits.

1. Introduction

The Paleocene-Eocene was characterized by a predominantly warm global climate (Kennett and Stott, 1991) lasting until the climatic cooling of the latest Eocene (Zachos et al., 2001). During this time, extensive Eocene carbonate platforms developed across three belts within the Neo-Tethys ocean (Scheibner and Speijer, 2008; Martín-Martín et al., 2025a, 2025b): the northern belt linked to the northern margin of the Neo-Tethys in Europe, the intermediate belt associated with microplates in the western Neo-Tethys, and the southern belt corresponding to the northern Africa-Arabia-India margins, extending from the Atlantic Domain to the southern margin of the Neo-Tethys. These platforms were rich in larger benthic foraminifera (LBF), ranging from inner to open oligophotic marine conditions. The presence of

* Corresponding author.
E-mail address: manuel.martin@ua.es (M. Martín-Martín).

https://doi.org/10.1016/j.sedgeo.2026.107055
Received 22 December 2025; Received in revised form 5 February 2026; Accepted 7 February 2026
Available online 9 February 2026

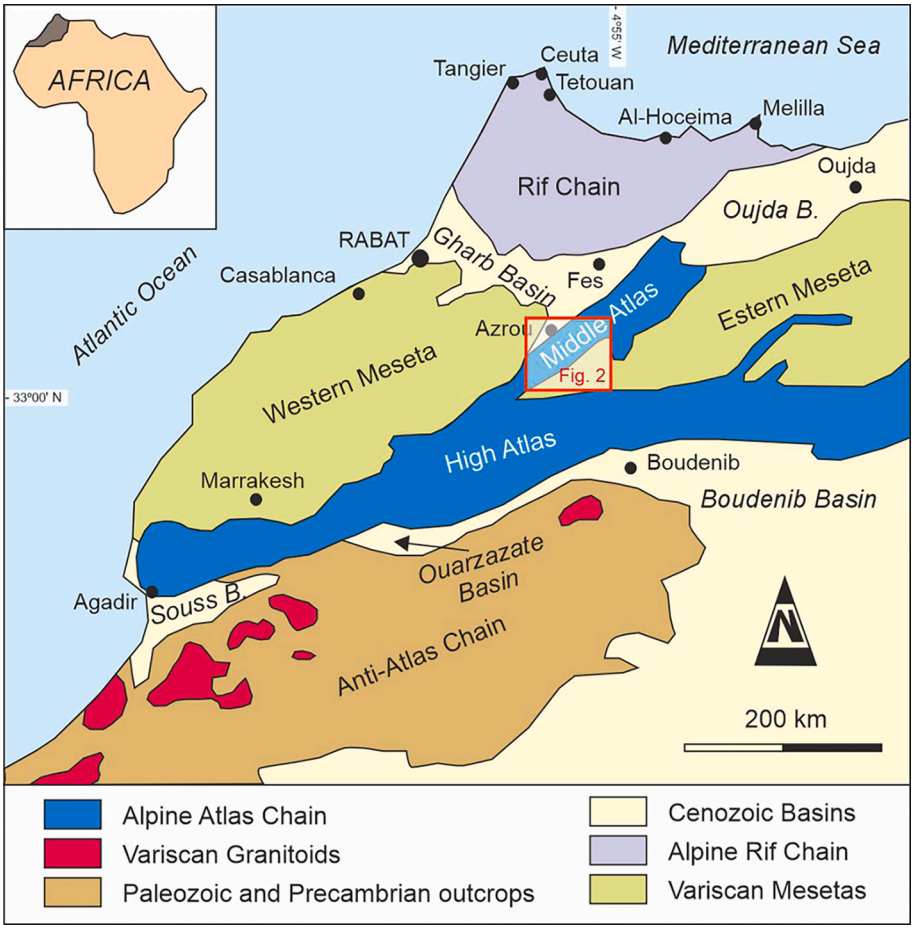

Fig. 1. General geologic map of northern Morocco, showing the location of the main domains (Rif, Mesetas, Atlas, and Anti-Atlas Chains, and Cenozoic basins) after Michard et al. (2008). The study area is highlighted in the Middle Atlas sector (Fig. 2).

interspersed seagrass and coralline algal maerl environments, along with coral patch-reef constructions (Nebelsick et al., 2005; Martín-Martín et al., 2001, 2020a, 2021, Martín-Martín et al., 2023a, 2023b, Martín-Martín et al., 2025a, 2025b, 2025c; Coletti et al., 2022; Tosquella et al., 2022, 2025; Talmat et al., 2025; Miclăuș et al., 2025), was also common.

In the case of northern Morocco, several key areas showing Paleogene platforms have been identified in relation to different structural domains. The following main structural domains are distinguished in this area (Fig. 1) (Michard et al., 2008): (1) the Neoproterozoic Pan-African belt, which outcrops in the Anti-Atlas as an anticlinorium, comprising a core of Precambrian and lower Paleozoic rocks and surrounding the northern portion of the Paleoproterozoic West African Craton; (2) the Variscan Western and Eastern Moroccan Mesetas composed of Paleozoic rocks; (3) the Alpine Middle and High Atlas, made up of Paleozoic to Paleogene rocks; and (4) the Alpine Rif Chain, consisting of Paleozoic to Miocene rocks. Several Miocene-Quaternary basins are underlain by this structural framework (Fig. 1), including the Gharb, Oujda, Souss, Ouarzazate, and Boudenib basins.

Two main sectors of Eocene carbonate platforms are described in the literature in northern Morocco: (1) Platforms influenced by the Tethys, rich in larger benthic foraminifera (LBF) and zooxantelate-corals, associated with the Ghomaride Internal Domain in the Rif Chain, spanning from the Tetouan to Al-Hoceima areas (Martín-Martín et al., 2023a, 2023b, 2025a, 2025b); and (2) Platforms influenced by the Atlantic, rich in phosphates, fish remains, and oysters, with an almost complete lacking of both larger benthic foraminifera and zooxanthellate corals. These platforms are located within the Sub-Atlas Group of the Middle and High Atlas Domains, extending from the Azrou to Agadir areas (Segonzac et al., 1986; Herbig, 1986, 1988, 1991, 1993, Trappe, 1991, 1992; Granier et al., 1997, 2002; Scheibner and Speijer, 2008: Amelieh et al., 2026). Similar facies to those in the second sector have also been recently reported in the Algerian-Tunisian Saharan Zone (Chadi et al., 2013; Kechiched et al., 2020; Boulemia and Adnet, 2023).

The Tethys-influenced Eocene platforms developed along the southern margin of the Mesomediterranean Microplate (Guerrera et al., 2021; Martín-Martín et al., 2020b, 2020c) within the southwestern branch of the westernmost Neo-Tethys. These platforms are notably rich in larger benthic foraminifera (LBF) and zooxantelate-corals (z-corals) (Martín-Martín et al., 2023a, 2023b, 2025a, 2025b). In contrast, the Atlantic-influenced platforms in Morocco developed in small, narrow basins along the western margin of North Africa. These platforms are characterized by rich assemblages of oyster reefs, fish remains, and coralline algae, yet they almost entirely lack LBF and z-corals (Segonzac et al., 1986; Herbig, 1986, 1988, 1991, 1993; Herbig and Gregor, 1990; Trappe, 1991, 1992; Granier et al., 1997, 2002; Scheibner and Speijer, 2008; Amelieh et al., 2026). This anomaly in Eocene carbonate platforms has been the subject of significant discussions and debates. The influence of cool, phosphate-rich waters from Athantic upwelling currents has been proposed as an explanation (e.g., Herbig, 1986; Scheibner and Speijer, 2008). The goal of this paper is the study of the Eocene carbonate platforms in the sector between Bekrit and Timahdite. The objectives of this work are: (1) to elucidate their paleoecological and paleoenvironmental evolution; (2) to identify the possible causes for the absence of LBF and the nearly nonexistent populations of z-corals; (3) to discuss the geodynamic and paleogeographic implications of these

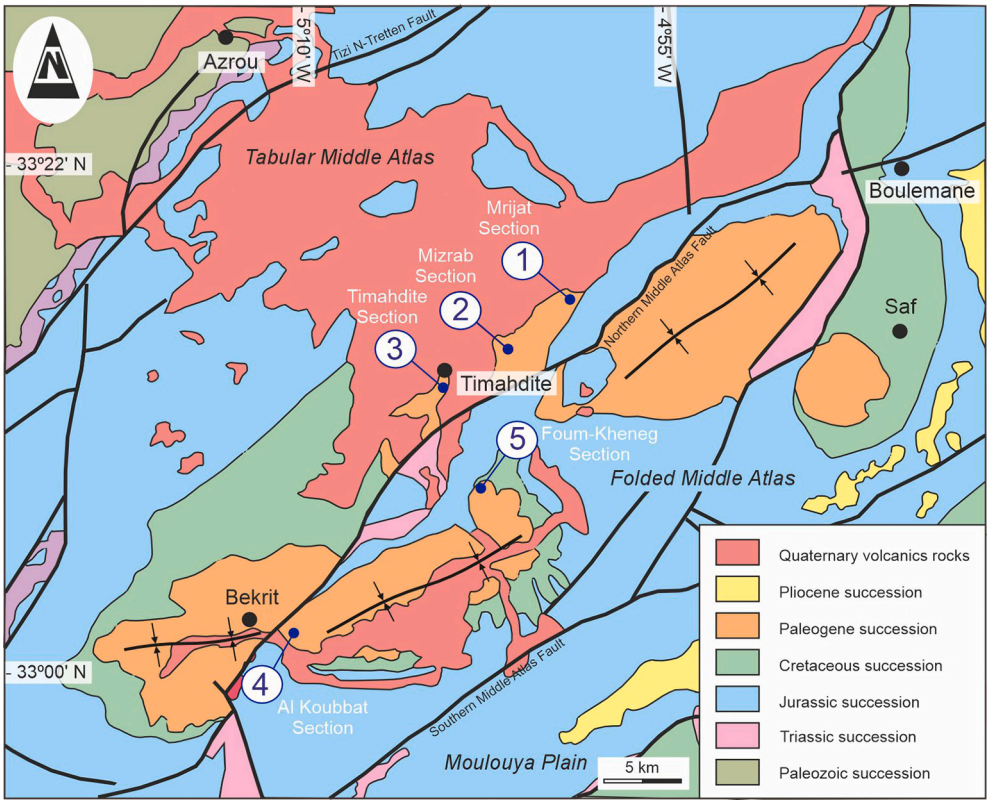

Fig. 2. Geological sketch map of the Bekrit-Timahdite sector in the Middle Atlas Domain, based on Duée et al. (1977), Fedan (1988), Charrière (1990), and Hinaje (2004), highlighting the locations of the studied sections.

findings; and (4) to correlate the studied platforms with coeval successions in the western-central Tethyan domain for explaining, in a regional context, the differences between the fossil assemblages between the Atlantic- and Tethys-influenced carbonate platform types. Based on this correlation, a possible cause for this anomaly is proposed.

2. Geological setting of the Bekrit-Timahdite sector

2.1. Structural setting

The Middle Atlas, part of the Atlas Mountain Chain, is an NE-SW intracontinental Alpine range (Choubert and Marcais, 1956; Michard et al., 2008; Amrani, 2016). It is bounded to the west by the Western Meseta and to the east by the Western and the Eastern Mesetas, both of them shaped by Variscan geological evolution. The structural composition features broad synclinal basins with axes aligned parallel to the range, combined with narrow anticlinal ridges that are occasionally intruded by granitic rocks (Colo, 1961; Fedan, 1988; Michard et al., 2008; Amrani, 2016). In the Bekrit-Timahdite sector (Fig. 2), the Middle Atlas is affected by several prominent faults, trending roughly SW-NE, resulting in the subdivision into several subdomains. The Tizi-N'Tretten Fault delineates the Western Meseta to the northwest from the Tabular Middle Atlas. Additionally, the Northern and Southern Middle Atlas Faults separate the Folded Middle Atlas to the northwest from the Tabular Middle Atlas and the Moulouya Plain to the southeast, respectively, thus connecting the Eastern Meseta (Termier, 1936; Colo, 1961; Duée et al., 1977; Fedan, 1988; Charrière, 1990; Hinaje, 2004). The study area shows Cretaceous-Paleogene successions adjacent to the Northern Middle Atlas Fault (NMAF). The Cenozoic structure in the Bekrit-Timahdite-Boulemane region consists of a syncline that is also influenced by the Northern Middle Atlas Fault. Additionally, there are other less significant faults, oriented approximately north-south, which further impact the geological landscape (Fig. 2). The geological framework is completed by Quaternary volcanic deposits and paleovolcanoes, predominantly outcropping in the Tabular Middle Atlas, but also present in the core of the Bekrit to Foum-Kheneg syncline within the Folded Middle Atlas subdomain (Mhyaoui et al., 2017; Benamrane et al., 2022).

2.2. Stratigraphic setting

The stratigraphic succession in the study area is represented by Paleozoic to Quaternary sedimentary deposits (Fig. 2). The Paleozoic basement primarily consists of detrital and carbonate deposits, outcropping in the Western Meseta, near Azrou. This basement is unconformably overlain by Triassic continental red-beds interspersed with doleritic balsalts (Lorenz, 1976; Mattis, 1977). The Jurassic System is characterized by carbonate platform facies with Tethyan affinity, while the Cretaceous consists of phosphatic marls, black shales, marly limestones, and gypsum-rich marly formations. The top of the Cretaceous deposits (Senonian) is defined by the El Koubbat Formation, according to Herbig and Fechner (1994). Overlying unconformably the Cretaceous, are Paleocene-Eocene deposits, representing carbonate platforms rich in gastropods, coralline algae, fish remains, and oysters (Segonzac et al., 1986; Herbig, 1986, 1988, 1991, 1993; Herbig and Gregor, 1990; Trappe, 1991, 1992; Granier et al., 1997, 2002; Scheibner and Speijer, 2008; Amelieh et al., 2026). They were defined as the Bekrit-Timahdite Formation (Herbig, 1991, 1993) of Thanetian to Lutetian age (Dragastan et al., 2012; Amelieh et al., 2026), though this age is still poorly constrained. Depending on the sector, the age of this formation can vary and may be restricted to the Ypresian-Lutetian (Herbig, 1988). Conformably overlying this formation, are shallow marine to continental post-Middle Eocene sediments of the Feleddi Formation made of gypsum-bearing red beds and lacustrine deposits (Herbig, 1993). The most recent deposits in the area include a Pliocene fluvio-lacustrine succession and Quaternary volcaniclastics (Mhyaoui et al., 2017; Benamrane et al., 2022).

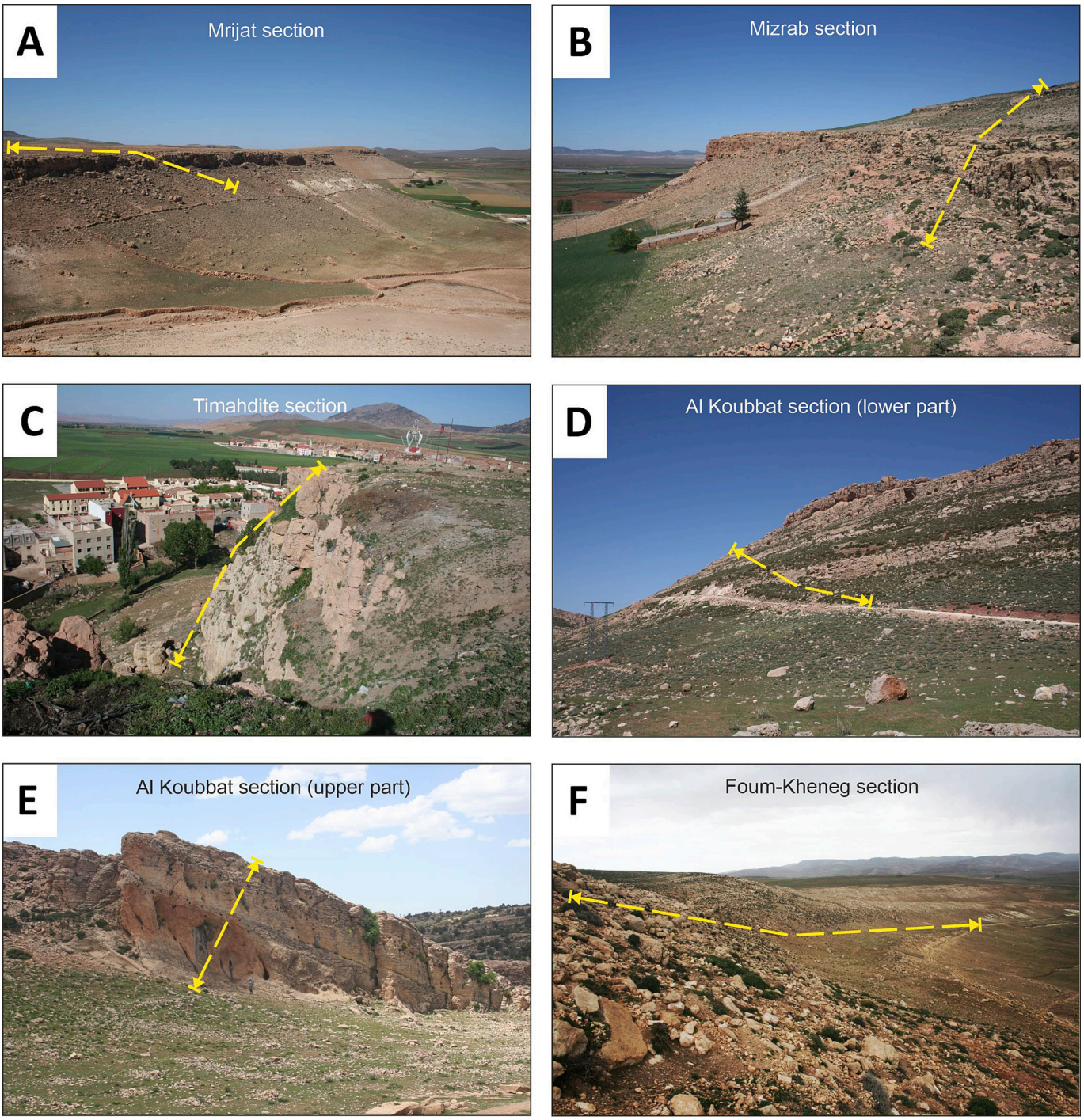

Fig. 3. Panoramic view of the studied sections in the Bekrit-Timahdite sector (Middle Atlas Domain) with the locations of the measured and sampled sections (yellow dashed lines): A) Mrijat section; B) Mizrab section; C) Timahdite section; D) Al Koubbat section (lower part); E) Al Koubbat section (upper part); F) Foum-Kheneg section.

3. Materials and methods

This study comprised both field and laboratory analyses. Field analyses involved logging and sampling, conducted according to standard procedures after removing the surficial cover, for microfacies analysis and biostratigraphic investigations. A total of 71 samples were collected from the studied sections (Fig. 3) of Mrijat (33°16′40”N /4°59′42”W), Mizrab (33°15′45”N/5°00′51”W), Timahdite (33°14′14”N/5°04′04”W), Al Koubbat (33°06′37”N/5°09′39”W), and Foum-Kheneg (33°09′23”N/5°03′17”W). Well-preserved rock samples were collected from each section, ensuring coverage of all identified field lithofacies. The sampling resolution was increased in areas where significant changes in sedimentary facies or fossil content were observed. Laboratory analyses focused on microfacies analysis and biostratigraphy, utilizing planktonic foraminifera, dinoflagellates, and calcareous nannoplankton for a comprehensive understanding of the stratigraphic context.

3.1. Microfacies analysis

Microfacies analysis was performed on 45 representative samples,

covering most of the identified field facies. Standard thin sections (2.0 × 3.0 cm) were prepared for examination to interpret paleoecological features and depositional paleoenvironments. Observations were made using a Nikon Eclipse E 200 optical microscope equipped with a Nikon DS-Fi2 digital camera system. Images were transferred to a PC via a Nikon's Digital Sight DS-U3 microscope camera controller and processed using the Nikon NIS Elements F4 imaging software. The analysis included the detailed description of lithology, grain type (skeletal/non skeletal), size and sorting, texture, fabric, and microfossil assemblages, following the methodology outlined by Flügel (2010). Microfacies classification was based on the terminology defined by Embry and Klovan (1971). To differentiate between microfacies assemblages, all allochem components and the matrix were systematically analyzed and visually estimated from the thin sections (Baccelle and Bosellini, 1965; Flügel, 2010).

3.2. Palynological analysis

A total of eight rock samples were processed for palynology: five from Foum-Kheneg (BT61–65), two from Al Koubbat (BT44, BT47), and one from Mrijat (BT1). Dinoflagellate cysts were recovered only from BT61, BT62, and BT63. The samples underwent standard palynological preparation (Hennissen et al., 2018; Riding, 2021), which included crushing the rock to approximately 500 μm, treating with hydrochloric acid (HCl) to remove carbonates, utilizing hydrofluoric acid (HF) to eliminate silicates, and applying hot HCl to remove fluorosilicates. The resulting kerogen was then sieved over a 20 μm mesh. Organic residues were stained with basic fuchsine when necessary and mounted in synthetic resin between glass slides and cover slips. Palynological slides were examined with a Nikon Eclipse 80i microscope, and the coordinates of all photographed specimens were recorded using an England Finder (EF) slide. Dinoflagellate cyst taxonomy was determined according to the most recent Lentin and Williams Index (Fensome et al., 2019). The first and last occurrences (FOs/LOs) of marker taxa for age determinations were compiled from published literature, prioritizing regional sources when available.

3.3. Planktonic foraminifera and calcareous nannoplakton analyses

To explore the potential content of planktonic foraminifera and other associated micropaleontological elements (primarily benthic foraminifera, radiolarians, and ostracods), 14 samples of marly sediments were collected (BT1 and BT6 from Log 1; BT42–45, BT47, and BT53 from Log 4; and BT61–65 and BT67 from Log 5). The samples were processed using the standard washing technique with sieves, retaining the >150 μm fraction for observation under a binocular microscope and subsequent picking of the specimens.

The smear slides for calcareous nannoplankton were prepared using the settling technique described by Flores and Sierro (1997). This method allows for homogeneous and comparable data analysis across samples, as well as enabling the estimation of the relative abundances of coccoliths. Specimen identification was conducted at 1000× magnification using a BK-POL-TR Trinocular Polarizing Microscope. For sample dating, the Paleogene biozonations of Okada and Bukry (1980) and Martini (1971) were followed.

4. Results

4.1. Lithostratigraphy

In the studied sections, 13 sedimentary facies (F1 to F13) were identified based on lithology, sedimentary structures (where visible), and fossil content. Their main features are detailed in the following paragraphs.

F1 – Chalky powdery deposits (Fig. 5A) are found in the Mrijat (samples BT1, BT3, BT6), Mizrab, and Al Koubbat sections (BT42, BT43, BT45, BT53). These deposits are loose and range in colour from white to reddish. Their thickness vary from 1 to more than 15 m. In thicker intervals within the Mrijat Section, interbeds of decimeter-thick calcarenite with parallel lamination, along with creamy limestones containing fossil gastropods (e.g., *Turritella*) are observed. In the Mizrab section, decimeter-thick dolomitized limestone layers are present, often accompanied by interlayers of marly limestone that may contain bivalves (e.g., cardiids and *Glycimeris*?) and echinoids. In the El Koubbat section, this facies is observed as interlayers (up to 1 m thick) between limestones rich in small fossil oysters and filament-like structures (likely juvenile oysters). In other cases, this facies is observed as thick deposits containing brain-shaped nodules of celestine.

F2 – Light gray mudstones are found exclusively in the Foum-Kheneg Section. They occur as a distinct unit in the lower part (BT61–63; BT67), which features decimeter-thick interbeds of limestone containing gastropods, and in the upper section. Also may appear as centimeter- to decimeter-thick interlayers within sandstones (BT64–65). These mudstones may also include subspheroidal sandy concretions. Characteristically laminated, their colour ranges from yellowish to gray. Siltier varieties are associed with sandstones units, although mudstones in the upper part of the succession are poorly exposed.

F3 – Limestones with gastropods (Fig. 5B and I) occur both as decimeter-thick interbeds within F1 and as bedded to massive units several meters thick across all sections. Their colour ranges from creamy to pink, reddish, or brownish. In certain beds within the Mrijat and Al Koubbat sections, *Turritella* specimens (Fig. 5J) measuring 4–5 cm in height were observed (BT4–5; BT46 respectively). Alongside gastropods, these limestones also contain bivalves, echinoid fragments or, in the Mizrab section, fish teeth. In El Koubbat, the limestone containing gastropods is classified as either algal limestones (with mainly codiaceans and dasyclades green calcareous algae) or calcareous bioclastic arenites, with the latter occasionally exhibiting parallel or cross laminations. Notably, some of the thicker units in the Mrijat section may also contain quartz grains or even clasts. In Foum-Kheneg, the limestone containing small gastropods may be oolithic (sample BT68 in Fig. 5C).

F4 – Limestones with bivalves are found in all sections, with a distinctive type identified in the El Koubbat section, characterized by large oysters. These limestones, displaying whitish, golden or pink colors may be oolithic or green-red algal (notably in Mizrab and Foum-Kheneg) and may contain, along with bivalves, small benthics, algae (mainly green and minorly rhodoliths) and filaments (thin-shelled bivalves), and, occasionally, echinoids or crabs. This facies may appear interbedded within chalky deposits (F1), exhibiting a white colour and soft texture. In the upper half of the El Koubbat section it is found as bedded bioturbated calcarenites (BT49–50) with parallel to cross laminations, as well as micritic limestones containing filaments, small gastropods, and echinoids (BT55).

F5 – Oyster limestones (Fig. 5D and K) are found only in the Al Koubbat section, where they form massive units several meters thick, composed of cemented, large, and robust shells in their living positions. Their coloration varies from creamy to pinkish to reddish (BT52). These limestones either overlie pseudobreccia containing large oysters or transition laterally into pseudobreccia.

F6 – Pseudobreccia with large oysters is observed exclusively in the Al Koubbatt section, occurring as beds of disorganised limestone clasts with oysters embedded in a soft, finer matrix (BT47; BT51) or free from any matrix. In the interval of 67–70 m, rough cross bedding can be observed.

F7 – Algal limestones occur as meters-thick beds of green (localy red) algal calcarenites in the Timahdite section (BT32–33), predominantly pink in colour. A similar facies is found in Mizrab, where it also contains small oysters and miliolids (BT23), while some light creamy varieties in the same section may additionally contain gastropods (BT29). In Mrijat, these limestones show interbeds of limestones (BT15–16) containing green (localy red as rhodoliths) algae (Fig. 5L) amidst red mudstones (F12).

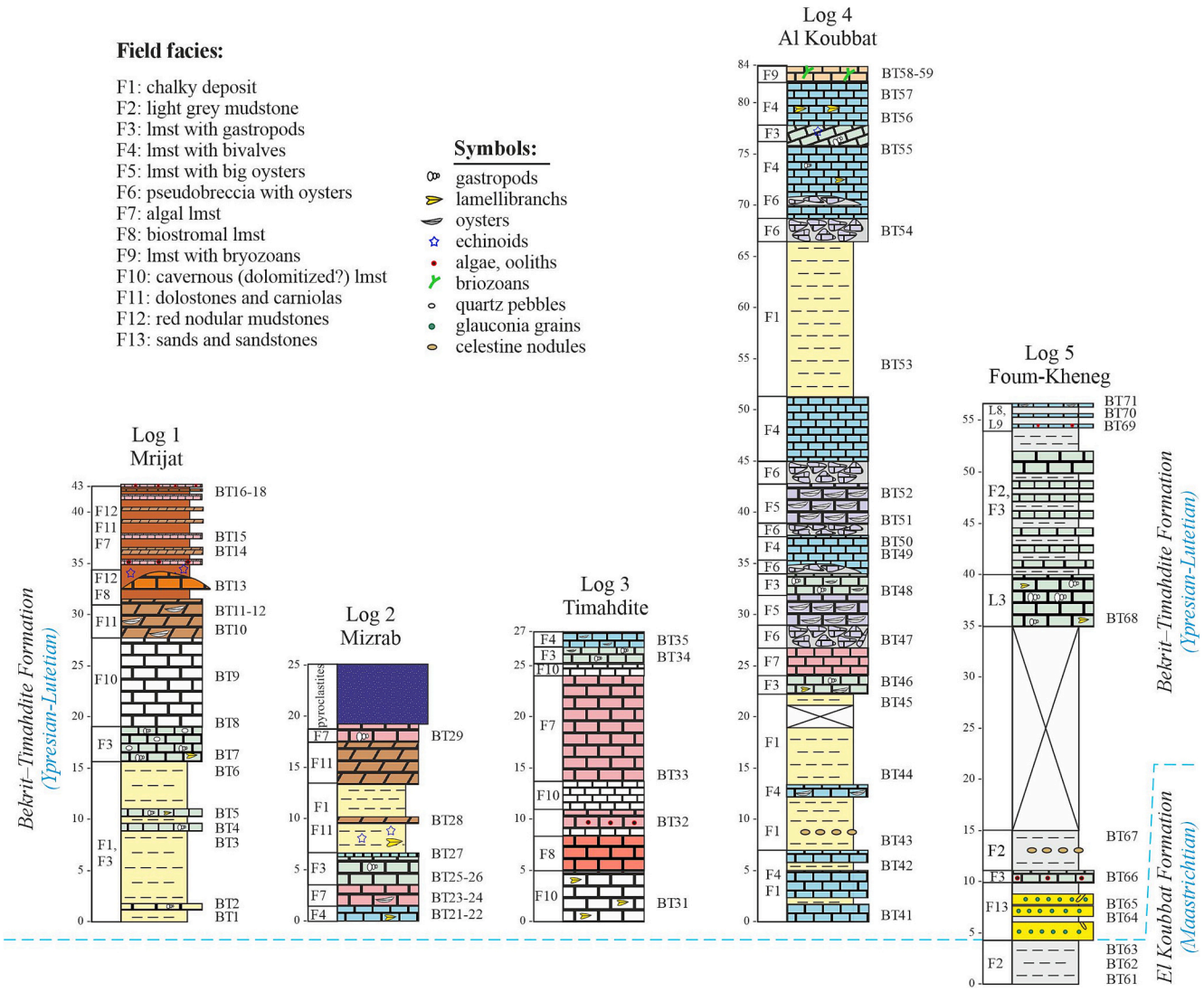

Fig. 4. Stratigraphic synthetic columns of the Bekrit-Timahdite sector illustrating the locations of the studied samples, defined field facies and fossil content. The dashed blue line separates the El Koubbat (Upper Cretaceous) and the Bekrit-Timahdite (Lower-Middle Eocene: Ypresian-Lutetian) formations.

F8 – Biostromal limestones (Fig. 5E) were observed in the Mrijat section and are considered questionable in Mizrab, where they might instead be classified as F7. These limestones consist of meter-thick, flat, lens-shaped bodies (BT13), mainly made of ostreids, algae and bryozoans as well as other microcomponents visibles in the thin sections, embedded within red mudstones (F12). The upper part features a red crust, 5–10 cm thick.

F9 – Reddish limestones with bryozoans (Fig. 5F) were identified exclusively in the uppermost 1 m of the sedimentary succession exposed in Al Koubbat. These red micritic limestones contains bryozoans (Fig. 5M), gastropods, and thin-shelled bivalves (BT58–59).

F10 – Cavernous (dolomitized?) limestones are primarily found in the Timahdite section, where the massive limestone exhibits dissolution voids of variable sizes. The original limestones may consist of creamy grainstones with small benthics (BT31) or a reddish coralline (biostromal) type. In Mrijat, this facies occurs as massive (BT9) to bedded (BT10) light tan limestones containing debris and impressions of echinoids.

F11 – Dolomite and carniolas (Fig. 5G) are predominantly observed in the Mrijat Section, with additional occurrences in Mizrab and Timahdite, where they can be difficult to differentiate from the cavernous limestones in the field. In Mrijat, the brown carniolas are overlain by reddish dolomites (BT11) characterized by interlayers of white diagenetic limestones (BT12). This facies may also occur as decimeter-thick interbeds within F12. These dolostones may feature echinoids fragments (Fig. 5N).

F12 – Red (nodular) mudstones (Fig. 5H) are associated with biostromal bodies (F8), mainly made of ostreids, algae and bryozoans, in the Mrijat section and contain interbeds of F7, F11. These mudstones may feature undeformed echinoids (Fig. 5O).

F13 – Sands and sandstones were observed only in the Foum-Kheneg section, consisting of fine glauconitic sands that range in colour from whitish to rusty. The upper meter is more or less cemented and bioturbated, showing *Skolithos* structures and may contain scattered shark teeth (Fig. 5P). The sands are crisscrossed by a network of fractures. Below the cemented sand, a half-meter interval is predominantly silty (BT64). A mudstone, less than 1 decimeter thick (BT65), divides the cemented interval into two nearly equal beds, with the upper bed featuring a coarse lag of teeth and fine rudites at the top.

4.2. *New biostratigraphic ages*

Biostratigraphic analysis provided limited but valuable results. All sections were extensively sampled for planktonic foraminifera, calcareous nannoplankton, and eight samples were analyzed for palynology. The search for planktonic foraminifera was unproductive, but

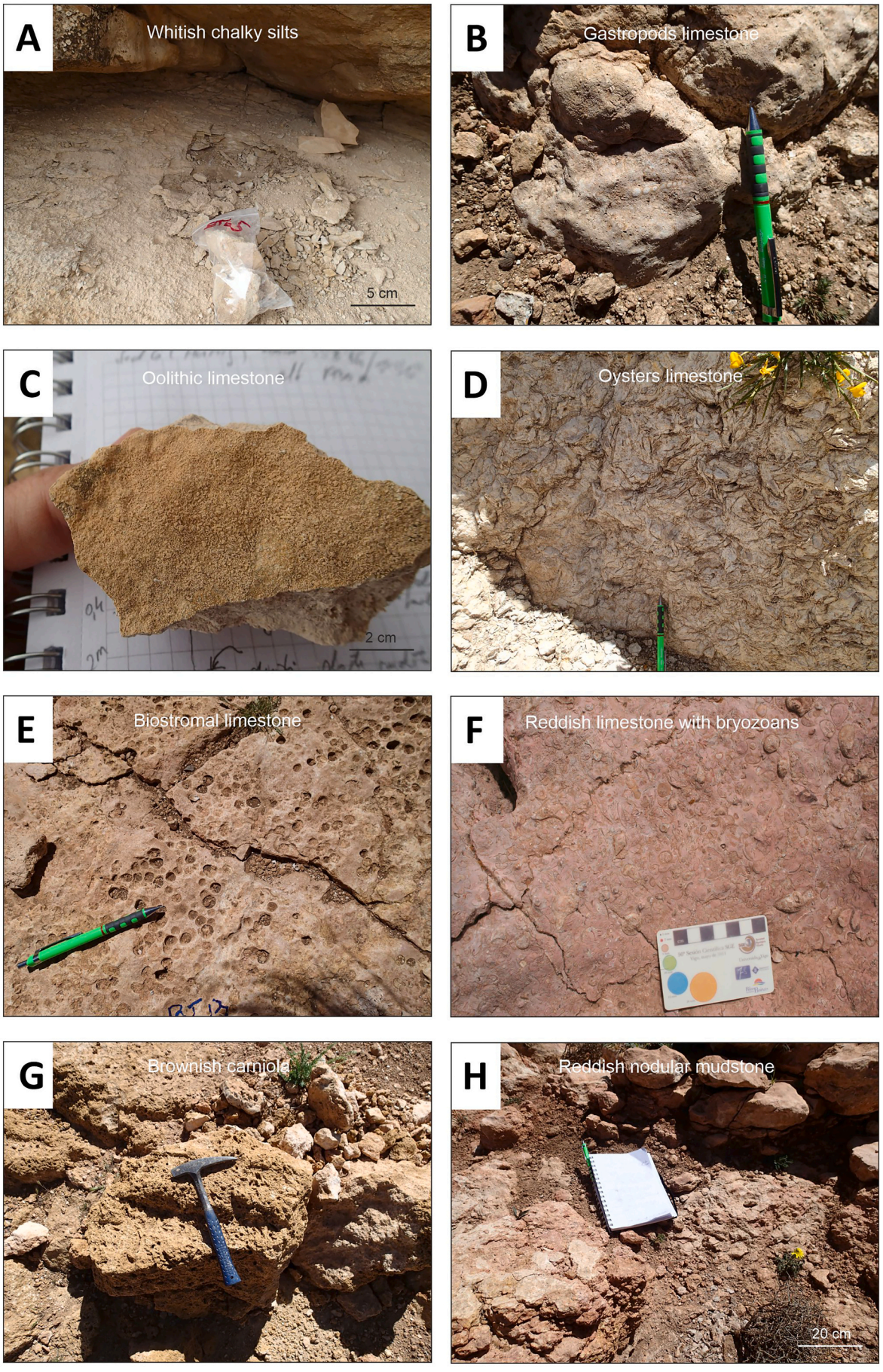
A
Whitish chalky silts
5 cm
B
Gastropods limestone
C
Oolithic limestone
2 cm
D
Oysters limestone
E
Biostromal limestone
F
Reddish limestone with bryozoans
G
Brownish carniola
H
Reddish nodular mudstone
20 cm

Fig. 5. Field lithofacies of the Bekrit-Timahdite sector (A to H): A) Whitish chalky powdery silts (F1); B) Limestones with gastropods (F3); C) Oolithic limestone with small gastropods (F3); D) Oysters limestone (F5); E) Biostromal limestone (F8); F) Reddish bryozoans limestone (F9); G) Brownish carniola (F11); H) Red nodular mudstone (F12). Fossil details in the studied sections (I to P): I) Aboundand gastropods in pinkish limestone (F3); J) *Turritella* in creamy limestones (F3); K) Limestone with big oysters (F5); L) Limestones with red algae: rhodoliths (F7); M) Bryozoans on pink limestones (F9); N) Echinoid fragments in dolostones (F11); O) Echinoid from red nodular mudstones (F12); P) Shark teeth in sandstones (F13).

calcareous nannoplankton and palynological content yielded positive results in some samples.

Palynological data from samples BT61 to BT63 in the lower Foum-Kheneg section indicates that the top of the El Koubbat Formation (Figs. 3F, 4, 5A) spans the late (but not terminal) Maastrichtian. These samples (Fig. 6A-F) contain *Senegalinium* spp., *Cerodinium* spp., and abundant *Areoligera senonensis* and *A. coronata*, all with first occurrences (FOs) in the late Campanian (Slimani et al., 2016, 2021). The assemblage also includes *Diphyes colligerum*, marking the early Maastrichtian (Chafai et al., 2024), along with late Maastrichtian species like *Andalusiella* spp., *A. mauthei* subsp. *mauthei*, *Cordosphaeridium fibrospinosum*, *C. exilimurum*, *C. eoinodes* subsp. *eoinodes*, *Lejeunecysta globosa*, *L. hyalina*, *Palaeocystodinium* spp., *P. australinum, Spiniferites membranaceus*, and *Xenascus* sp. (Powell, 1992; Chakir et al., 2020; Jbari et al., 2020; Slimani et al., 2021; Jbari and Slimani, 2022). The presence of *Hafniasphaera fluens* in BT63 suggests a latest Maastrichtian age (Hansen, 1977; Hansen, 1979). However, the lack of the *Manumiella seelandica* acme, an indicator of the terminal Maastrichtian, indicates that the latest Maastrichtian is missing in this section (Rauscher and Doubinger, 1982; Slimani et al., 2010; Guédé et al., 2014). The continuous presence of *Dinogymnium*, which last occurs in BT63, aligns with its extinction at the Cretaceous–Paleogene (K–T boundary (Guédé et al., 2014; Slimani et al., 2010; Chakir et al., 2020; Jbari et al., 2020). Finally, the absence of Paleocene markers like *Carpatella cornuta* and *Danea californica* rules out a Paleocene age (Guédé et al., 2014).

The overlying Bekrit–Timahdite Formation in the lower Foum-Kheneg section (samples BT64–65) is dated to the middle Lutetian (CP12–13 of Okada and Bukry, 1980 NP14–15 of Martini, 1971) based on calcareous nannoplankton, notably *Nannotetrina fulgens* (Fig. 6G–I).

Biostratigraphic data reveal a significant hiatus spanning from the terminal Maastrichtian to the middle Lutetian. Overlying this gap, the Paleogene consists of glauconitic sands with shark teeth interbedded in marls, suggesting a transgression (Fernández-Landero and Fernández-Caliani, 2021; Tribovillard et al., 2023) after a major sea-level drop that caused subaerial exposure and erosion at the K/T boundary. This finding is consistent with El Attmani et al. (2021) in the Foum-Kheneg region, where sequence stratigraphy identifies two distinct bio-sedimentary systems, the Campanian–Maastrichtian system and the Paleogene system, separated by a sequence boundary of regional significance, identifiable in the Morocan Meseta basins.

We were unable to obtain age data for the samples collected from the other studied sections. Therefore, in this study, based on our data and literature (Geyer and Herbig, 1988; Herbig, 1991, 1993; Granier et al., 1997, 2002; Scheibner and Speijer, 2008: Mebrouk et al., 2009; Dragastan et al., 2012; El Attmani et al., 2021; Amelieh et al., 2026), we assign an Ypresian-Lutetian age to the Bekrit-Timahdite Formation, although this age remains poorly constrained.

4.3. Microfacies description

Oyster and other bivalves are common in the examined materials, contributing to the oyster-rich levels of facies F4, F5 and F6. Furthermore, they are chiefly scattered as distinctive components in diverse carbonate textures throughout most thin sections from other facies. Other significant macrofossils, such as gastropods (lithofacies F3), green algae (codiaceans and dasyclads; F7), bryozoans (F9), and echinoid plates and spines, are widely represented across most facies. Together, they constitute the major components of the fossil assemblage observed in the studied deposits. In all instances, the sample washings yielded no planktonic foraminifera. The most frequently identified organic components were ostracods and fish remains, which were particularly abundant in BT61 and BT63 to BT65. To a lesser extent, bivalve and gastropod remains were also commonly observed, while sponge spicules and echinoderm remains appeared less frequently, mainly in BT1 and BT53. Only occasionally, in some samples (BT1, BT6, BT67) a benthic foraminiferal oligofauna, consisting of very few, very small specimens was constated. In BT67, there was a noticeable abundance of ooid-shaped grains (ooliths). Furthermore, the general absence of charophyte (oogonia) remains suggests a lack of significant freshwater inputs during the sedimentation of the marly deposits.

From the analysis of the thin sections, eigth microfacies (Mf1 to Mf8) were identified in the studied Eocene sections (Table 1). Fig. 7 shows general views of the eight defined microfacies in the photos A to H, while in the photos I to P details of the fossil content are shown.

Mf1 is an azoic dolostone that underlies 'carniola-like' deposits in the field (samples BT8–9; F10).

Mf2 (F3, F4, F7, F10) shows a dolomitic grainstone texture with a moderately to well-sorted fabric primarily composed of skeletal remains, including disarticulated bivalves (30%), gastropods (15–20%), green algae (dasyclads and codiaceans; 15–20%), peloids (10–15%), ostracods (5–10%), miliolids (5–10%), and small quartz grains (5–10%). Other notable components include echinoid debris (2–5%), bryozoans (2–5%), and annelids (2–5%), with a significant portion of the skeletal grains being superficially micritized (cortoids). Locally, this microfacies develop a paleocaliche appearance, characterized by paleospeleothems infilling cavities. It can occasionally develop a micro-breccia aspect, where millimetric-sized, dark-colored intraclasts disrupt the original fabric.

Mf3 (F7) is a quartzarenite with a moderately sorted fabric that contains mollusk debris, mainly consisting of ostreids and other bivalves (15–20%), gastropods (10–15%), thin-walled ostracods (10%), and miliolids (2–5%).

Mf4 (F4) displays a wackestone texture with a moderately sorted fabric, in which common ostreids (15–20%) are isolated within a lime matrix, with a low diversity of fossils, mainly ostracods (5%), intraclasts (5%), and unidentified small benthic foraminifers (2–5%). Small quartz grains (5–10%) are commonly present.

Mf5 (F3, F4, F7) reveals a well-sorted grainstone texture, where disarticulated bivalves (mainly ostreids) are among the most abundant elements (25–30%), in addition to gastropods (5–10%), miliolids (10–15%), green algae (mainly dasyclads at 10–15%), branching bryozoans (10%), peloids (5–10%), ostracods (5%), intraclasts of warty to lumpy rhodoliths (*Sporolithon*, $\phi > 10$ mm, 5%), lithoclasts (2–5%), and small-sized quartz grains (2–5%). Other components include textulariids (2–3%), rotaliids (2–3%), unidentified small benthic foraminifers (2–3%), and annelids (2–3%). A significant portion of the skeletal grains show signs of micritization on their surface (cortoids).

Mf6 (F4, F7, F8, F11) is characterized by a well-sorted oolitic grainstone in which codiaceans (15–20%), dasyclads (10%), miliolids (10–15%), and cellariform bryozoans (10–15%) are the main components, along with common mollusk remains of gastropods (10–15%) and bivalves (mainly ostreids, 10–15%), echinoid debris (5–10%), peloids (5–10%), textulariids (2–3%), rotaliids (2–3%), ostracods (2–3%), spirorbid annelids (2–3%), rhodoliths (2–3%), small-sized quartz grains (2–3%). A significant portion of the skeletal grains is superficially micritized (cortoids).

Mf7 (F3, F4, matrix of F5–6) is a mollusk-dominated packstone with a moderately-sorted fabric, featuring a substantial presence of echinoid

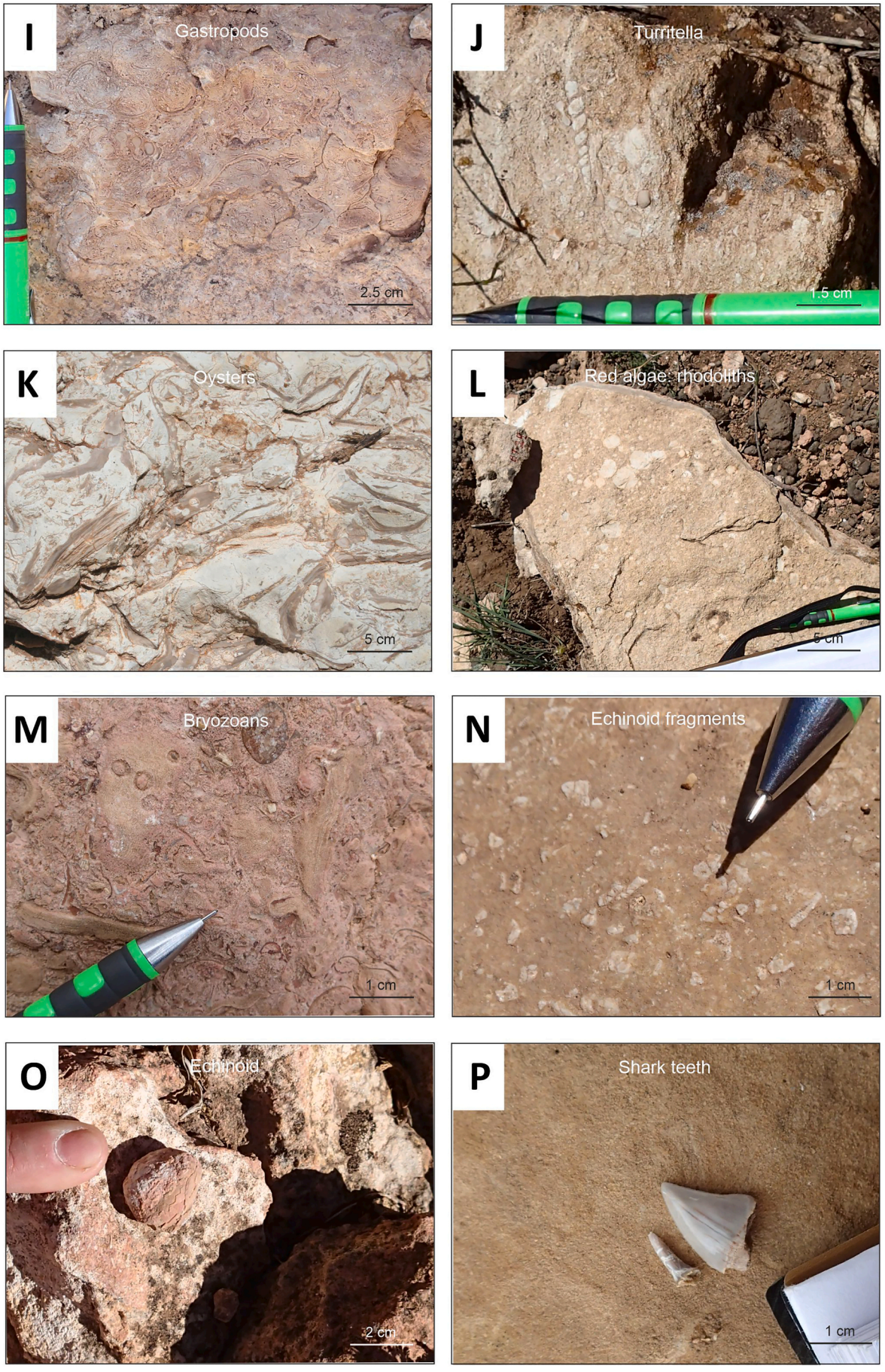

Fig. 5. (*continued*).

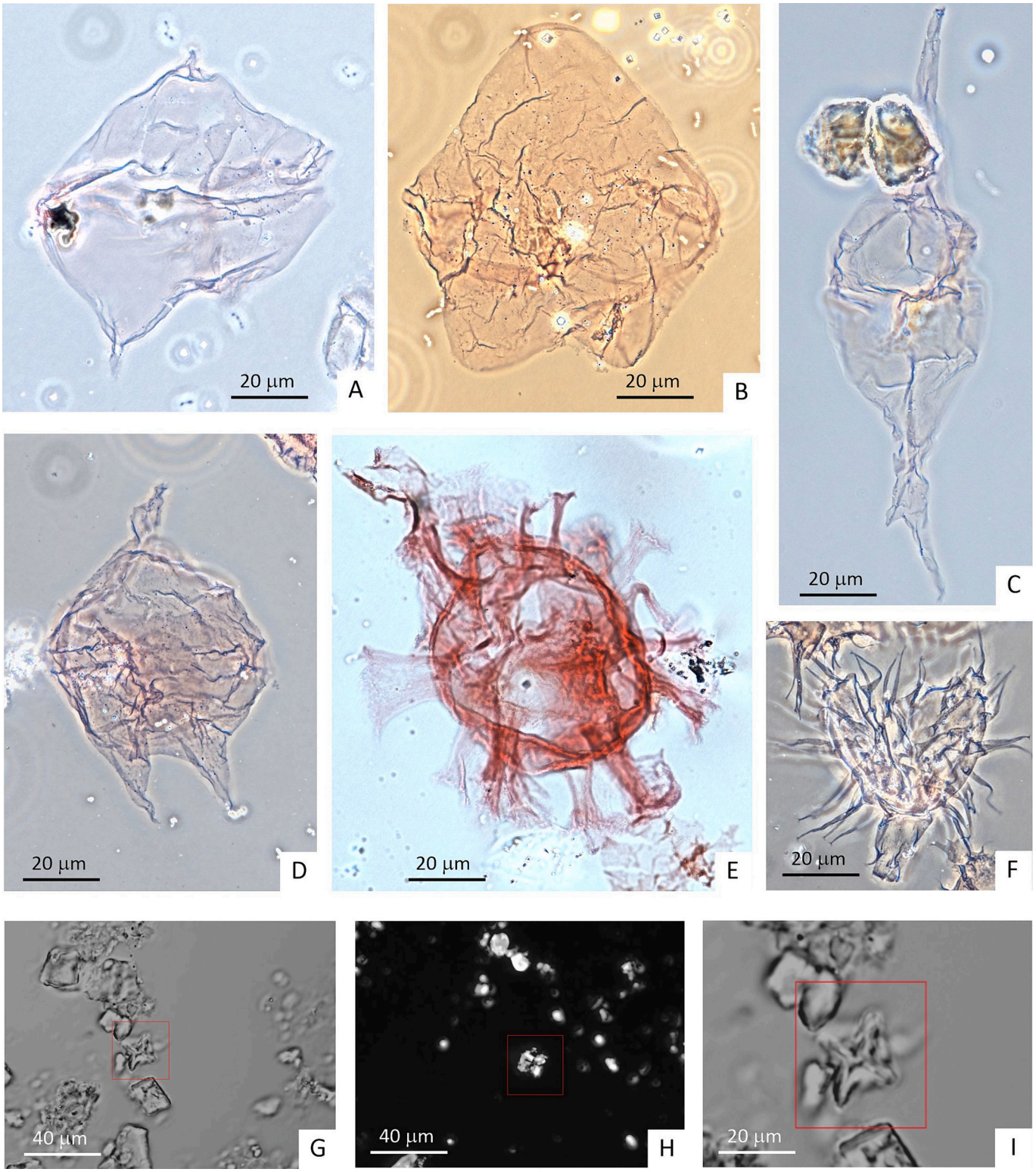

Fig. 6. Microphotos of dinoflagellates (A to F) and calcareous nannoplankton (G to I). A to F are taken in phase contrast, except for image (E), which was captured in interference contrast (scale bar is 20 µm for images A to F and I 40 µm for G and H): A) *Lejeunecysta hyaline* (BT63); B) *Lejeunecysta globosa* (BT63); C) *Palaeocystodinium australinum* (BT63); D) *Senegalinium bicavatum* (BT63); E) *Cordosphaeridium eoinodes* subsp. *eoinodes* (BT63); F) *Diphyes colligerum* (BT63); G) *Nannotetrina fulgens* (BT64); H-I) *Nannotetrina fulgens* (BT65).

plates and spines (20–25%). The main framework of this microfacies consists of gastropods (15–20%), ostreids (5–10%) and other bivalves (5–10%), often affected by bioerosion. Additional common components include ostracods (2–5%), peloidal intraclasts (2–5%), peloids (2–3%), textulariids (2–3%), miliolids (2–3%), rotaliids (2%), green algae (2%), bryozoans (2%), serpulids (2%), unidentified small benthic foraminifers (2%), and small quartz grains (2–5%).

Mf8 (F4, F9) is characterized by a moderately sorted fabric with

Table 1
Diagnostic characteristics of the identified microfacies, their correspondence with field lithofacies, and depositional environment interpretations.

Micro-facies (Mf)	Samples (BT) and field facies (F)	Description	Fossil and other components common and/or abundant (*)	Fossils and other components present and/or rare	Depositional environment
Mf1	8–9 (F10)	Fine-grained dolostone	Azoic	Isolate quartz grains	Supratidal environment
Mf2	29(F7), 31(F10), 66 (F3), 68 (F3), 69–71 (F4)	Dolomitized mollusk packstone-grainstone	Ostreids*, thin-shelled bivalves*, gastropods*, green algae*, ostracods, miliolids, peloids, cortoids, fine-sized quartz grains	Echinoid plate and spines, annelids, bryozoans	Intertidal to subtidal Inner ramp environment
Mf3	46 (F3)	Mollusk-rich quartzarenite	Rounded fine-sized quartz grains*, ostreid and other bivalve remains, gastropod fragments, ostracods	Miliolids	Subtidal Inner ramp environment
Mf4	41 (F4)	Ostreid wackestone	Ostreids*, ostracods, intraclasts, and rounded fine-sized quartz grains	Unidentified small benthic foraminifers	Deep-lagoon deposits Inner ramp environment
Mf5	21(F4), 23–24 (F7), 25–27 (F3), 33 (F7), 49 (F4)	Bivalve-rich grainstone	Ostreids*, thin-shelled bivalves*, miliolids*, dasyclad and codiacean algae*, gastropods, bryozoans, ostracods, peloids, cortoids, echinoid debris, rhodolith intraclasts, lithoclasts, rounded fine-sized quartz grains	Textulariids, annelids, unidentified small benthic and planktic foraminifers	Reworked ostreid-banks in back-shoal deposits Inner ramp environment
Mf6	10–12 (F11), 13 (F8), 14 (F11), 15 (F7) 16 (F7), 18 (F7), 32 (F7), 50 (F4)	Green algae oolitic grainstone	Dasyclad and codiacean algae*, bryozoans*, miliolids*, gastropods, ostreids, thin shelled bivalves, echinoid debris, peloids, cortoids	Textulariids, rotaliids, ostracods, spirorbids, rhodolith grains, fine-sized quartz grains	Shoal/channel deposits Inner ramp environment
Mf7	4–5 (F3), 7 (F3), 17 (F4), 22 (F4), 34 (F3), 35(F4), 48 (F3), 52(F5), 54 (F6), 55 (F4)	Mollusk and echinoid packstone	Echinoid debris*, gastropods*, thin shelled bivalves*, ostreids*, ostracods, textulariids, miliolids, peloidal intraclasts, fine-sized quartz grains	Green algae, rotaliids, annelids, bryozoans, unidentified small benthic foraminifers	Open marine deposits Inner-to-mid ramp environment
Mf8	56–57 (F4) 58–59 (F9)	Bryozoan packstone with echinoids and mollusks	Branching (adeoniform/ cellariform) and massive celleporiform bryozoans*, echinoid plates and spines*, gastropods*, ostreids*, annelids, ostracods	Miliolids, codiacean algae, unidentified small benthic foraminifers, fine-sized quartz grains	Open marine deposits Proximal mid ramp environment

abundant branching adeoniform and cellariform (10–15%) and massive celleporiform (10–15%) bryozoan colonies, as well as a significant presence of echinoid plates and spines (20%), ostreids and other bivalves (20–25%), gastropods (10–15%). Other common elements include serpulids (5%), ostracods (2–5%), codiaceans (2–3%), miliolids (2–3%), and unidentified small benthic foraminifers (2–3%) with small quartz grains (2–3%) also occasionally present.

5. Discussion

5.1. Paleoenvironmental evolution

Based on the analysis of the washed residue it can be concluded that the samples originate from sediments deposited in coastal lagoon environments, characterized by marsh-like conditions, with variable salinity. The oyster-rich calcareous intercalations most clearly reflect marine episodes, while the more marly levels, from which these samples were collected, indicate either regressive episodes or the establishment of lagoons isolated from the open sea by the oyster-bearing reefs themselves. The absence of charophytes suggests that these lagoons did not receive significant inputs of freshwater. Oysters, as sessile suspension-feeder bivalves, are highly tolerant of varying physical and ecologic parameters; they can thrive in environments ranging from brackish to normal marine waters and can inhabit both on hard and soft substrates (sand/mud). They can develop either in isolation or by cementing themselves to the substrate or to each other, forming banks or bioherms (Parras and Casadío, 2002, 2005; Toscano et al., 2018; Kassab et al., 2021; Ekin, 2024). Microfacies analysis allows the interpretation of paleoenvironments using a ramp model according to the terminology of Burchette and Wright (1992), Pomar (2001), and Pomar et al. (2017). Based on the data presented in Table I and Figs. 7 and 8, the azoic fine-grained dolostone microfacies Mf1 likely represents a supratidal setting within a sabkha-like environment, as suggested by the overlying presence of 'carniole' deposits. Both carniola deposits and dolostones are primarily associated with the precipitation of Mg-carbonate minerals, typically linked to microbial activity in saline environments, alongside other evaporitic minerals (El-Omla and Aboulela, 2012; Mohammed et al., 2022; Sánchez-Román et al., 2025). Mf2, a dolomitized mollusk packstone-grainstone, is interpreted as high-energy proximal lagoon deposits located in an intertidal-subtidal setting, possibly influenced by continental freshwater inputs (Powell and Moh'd, 2011). Mf3 microfacies, characterized by mollusk-rich quartzarenite, likely represents subtidal deposits in the innermost part of the lagoon, affected by terrestrial sedimentary inputs. Mf4, with its ostreid wackestone fabric, could represent deepest lagoon deposits within a muddy-substrate inner ramp environment (Buxton and Pedley, 1989; Flügel, 2010). Mf5, a bivalve-rich grainstone-packstone, characterized by a predominance of ostreids and miliolids, along with remains of other bivalves, gastropods, echinoids, dasyclades and codiacean algae, peloids and cortoids, is interpreted as reworked ostreid bioherm deposits accumulated in back-reef lagoonal settings subsequently to high energy storm events. These facies align with the "sand shoals and banks" microfacies type described by Flügel (2010). Mf6, a green algae oolitic grainstone microfacies, is often found situated in the upper part of these sequences. It consists primarily of dasycladae and codiacean algae, cellariform bryozoans, miliolids, and reworked ostreid remains. This microfacies is interpreted as deposits from shoal or tidal channel situated between ostreid bioherms in the distal part of the inner ramp (Flügel, 2010; Abdelhady et al., 2019; Abd El-Moghny and Afifi, 2022). Mf7 and Mf8 microfacies, characterized by a predominance of gastropods, bivalves, cellariform and celleporiform colonies of bryozoans, along with abundant echinoid plates and spines, are interpreted as transgressive deposits in open

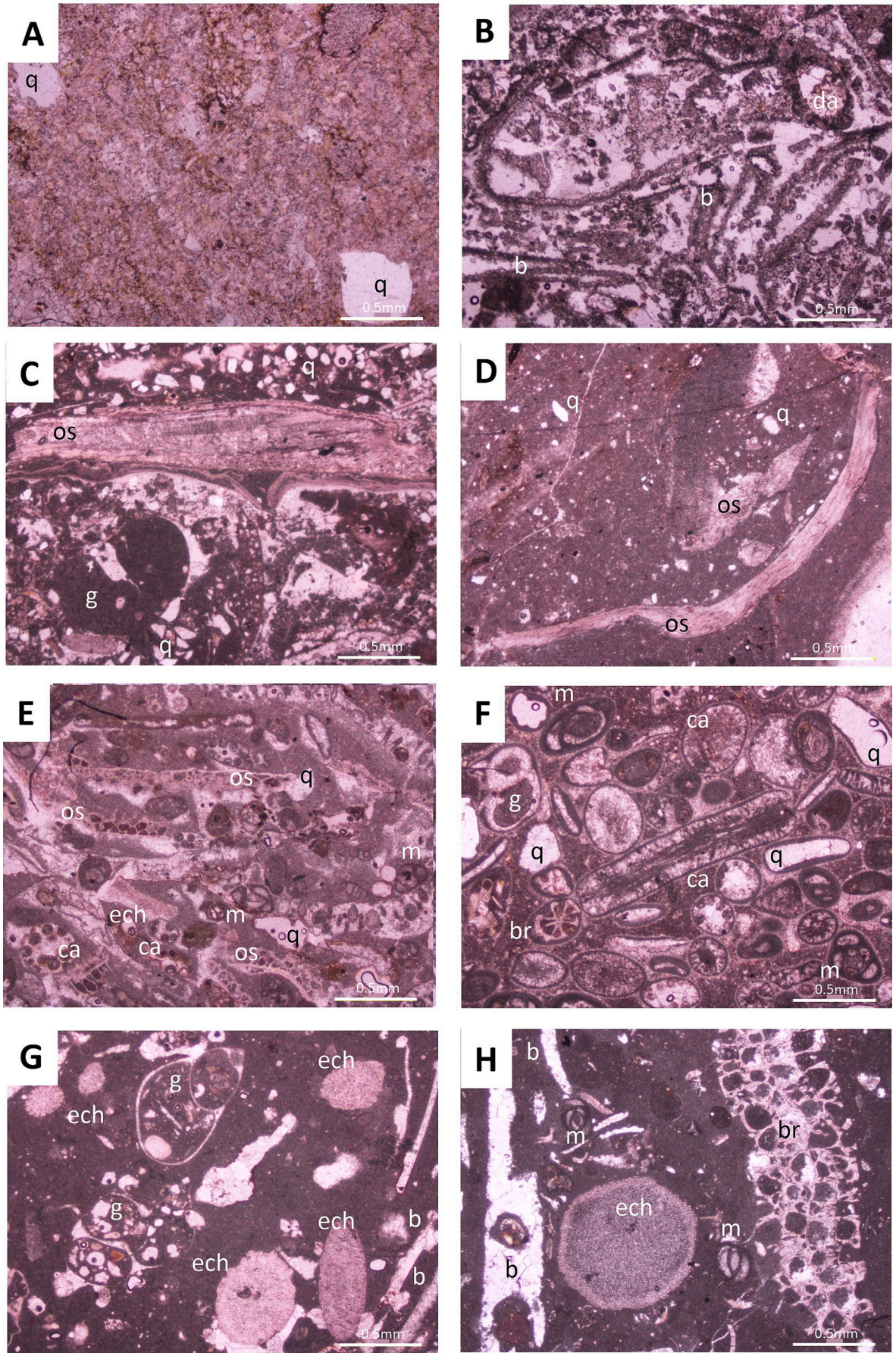
A
q
q
0.5mm
B
da
b
b
0.5mm
C
q
os
g
q
0.5mm
D
q
q
os
os
0.5m
E
os
q
os
m
ech
m
q
ca
ca
os
0.5mm
F
m
ca
q
g
q
q
ca
br
m
0.5mm
G
ech
g
ech
g
ech
b
ech
b
0.5mm
H
b
m
br
ech
m
b
0.5mm

Fig. 7. Photomicrographs of the main Eocene microfacies (A-H) and their main fossil components (I-P): A) **Mf1** (supratidal environment), BT8 (log 1, Mrijat section); B) **Mf2** (intertidal-to-subtidal deposits, inner ramp), BT69 (log 5, Foum-Kheneg section); C) **Mf3** (subtidal deposits, inner ramp), BT46 (log 4, Al-Koubbat section); D) **Mf4** (deep-lagoon deposits, inner ramp), BT41 (log 4, Al-Koubbat section); E) **Mf5** (back-shoal deposits, inner ramp environment), BT21 (log 2, Mizrab section); F) **Mf6** (shoal deposits, inner ramp), BT13 (log 1, Mrijat section); G) **Mf7** (open marine deposits, inner-to-mid ramp), BT3 (log 1, Mrijat section); H) **Mf8** (open marine deposits, proximal mid ramp), BT59 (log 4, Al-Koubbat section). I) Rhodolith intraclast (BT26, log 2; J) Detailed photomicrograph of the previous sample; K) Spirorbid and bryozoan assemblage (BT10, log 1); L) Green algal (mainly codiacean algae) oolithic grainstone (BT12, log 1); M) Mollusk packstone of ostreids and other undifferentiated bivalves (BT17, log 1); N) Mollusk packstone of ostreids and pectinids (BT22, log 2); O) Mollusk (bivalves and gastropods) and bryozoan packstone (BT56, log 4); P) Bryozoan packstone encrusting annelids (BT59, log 4). Scale bars: 0.5 mm (A-H, J-P) and 1 mm (I). Key: an, annelid; b, undifferentiated bivalve; br, bryozoa; ca, codiacean algae; ech, echinoid plates and/or spines; da, dasyclad algae; g, gastropod; m, miliolid; os, ostreid; pc, pectinid bivalve; q, quartz grain; ra, red algae (*Sporolithon* sp.); sp, spirorbid (annelid).

marine settings, specifically at the transition between the inner and the mid ramp. Across all the studied sections, the succession of microfacies suggests the presence of transgressive sequences (T). Oyster limestones are characterized as oyster-dominated deposits forming organic structures (build-ups) or prominent reliefs (mounds) that protect potential lagoons. Green algae, particularly codiaceans and dasyclades, also represent one of the most prominent groups found colonizing protected environments such as marine lagoons (Milliman, 1974; Wray, 1977; Burollet, 1981; Shili et al., 2002; Granier, 2012). Their co-occurrence with miliolids, which are characteristic of warm marine waters with low turbulence, sometimes under slightly hypersaline conditions (Hallock and Glenn, 1986; Murray, 2006; Roozpeykar and Moghaddam, 2016; Chan et al., 2017; Sarkar, 2019), supports this environmental context. Bryozoans represent another major component of marine environments primarily characterized by abundant cellariform and celleporiform colonies mostly prevalent in circalittoral marine environments (Moissette, 2000; Bialik et al., 2023). This is reinforced by the higher presence of echinoid plates and spines.

5.2. Ramp facies rims, carbonate factories, trophic and photic conditions

A combination of photozoan and heterotrophic elements has been found in the fossil assemblage of the studied Eocene sedimentary succession. The photozoan association is mostly constituted of abundant green algae (dasyclades and codiaceans) which primarily indicate protected, shallow warm waters in low-to-mid latitudes (Milliman, 1974; Wray, 1977; Granier, 2012). The heterotrophic assemblage, in turn, consists of small benthic (miliolids, textulariids, rotaliids) and planktonic foraminifers, mollusks (including ostreids, other bivalves, and gastropods), echinoids, bryozoans, annelids, ostracods, and various filter-feeding organisms. Photozoan and heterotrophic assemblages suggest nutrient availability in meso- to eutrophic habitats influenced by nearby upwelling and/or terrestrial riverine inputs in the area (Herbig and Gregor, 1990; Dragastan and Herbig, 2007; Michel et al., 2011, 2019). Additionally, intense bioerosion has been observed on mollusk shells. All the above features suggest inner ramp marine environments (Burchette and Wright, 1992), which are "dominated by sand shoals or organic barriers and shoreface deposits, and back-barrier peritidal areas" with euphotic conditions, characterized by meso- to eutrophic waters (Hallock and Schlager, 1986; Hallock, 1988; Barbosa et al., 2021). The potential existence of non-evergreen seasonal (algal-like) seagrass meadows within the Eocene sediments is also conceivable. Generally, seagrass-related facies are characterized by heterometric and unsorted grain-dominated sediments with a variable content of mud (Mateu-Vicens et al., 2012; Brandano et al., 2019; Baceta and Mateu-Vicens, 2022). Shoal and back-shoal deposits (microfacies Mf5 and Mf6), are likely the result of reworking by currents and/or high energy events (storms) of a seasonal seagrass meadow located landward of an ostreid-bioherm mound, concentrated due to the baffling and trapping effects (Mateu-Vicens et al., 2012; Reich et al., 2015; Baceta and Mateu-Vicens, 2022). Additionally, the frequent occurrence of miliolids, along with common textulariids and rotaliids, as motile and grazing foraminifers, is often related to nutrient-rich plant microhabitats, such as rhizomes of both phanerogams and seagrasses (Mateu-Vicens et al., 2014; Reich et al., 2015; Tomassetti et al., 2016). The presence of mollusks, ostracods and predominantly branching colonies of bryozoans also support this interpretation (Moissette, 2012; Reich et al., 2015). Finally, the concurrent occurrence of echinoids in the assemblage aligns with euphotic subtidal seagrass environments in the inner ramp (Flügel, 2010; Mateu-Vicens et al., 2012; Baceta and Mateu-Vicens, 2022). Microfacies Mf7 and Mf8 are characterized by a dominance of cellariform and celleporiform bryozoans, often assigned to upper circalittoral settings (Moissette, 2000). The abundance of echinoid plates and spines also suggest an open marine environments at the transition with the mid ramp (Flügel, 2010). However, the presence of reworked rhodolith (*Sporolithon*) gravel pebbles in shoal deposits would indicate the development of coeval or slightly older maërl ecosystems in deeper mesophotic mid ramp environments (Coletti and Basso, 2020), which are not represented in the sedimentary record of the area. Sporolithaceans are typically found in low latitude, and most of the authors suggest not very deep- to deep-water settings (Aguirre et al., 2000; Coletti and Basso, 2020). Our sedimentary reconstruction is comparable to the idealized Tertiary ramp profile presented by Buxton and Pedley (1989), illustrating proximal to distal facies rims.

From the carbonate *"factory"* point of view, the proposed ramp parallels the heterozoan warm-water carbonates model described by Westphal et al. (2010), Michel et al. (2011) and Michel et al. (2019). It specifically reflects the photozoan-heterozoan transition (showing partial similarities with the 'C-factory'), characterized by the presence of up to 20% photozoan components within a heterozoan sediment, suggesting warm temperatures and nutrient-rich conditions, also supported by the presence of ooids, peloids and cortoids (Schlager, 2003; Flügel, 2010). In the same time, the abundant algal content links these deposits to the green algae–foralgal assemblage (GA-foralgal; Brandano et al., 2019), which is typical of tropical seagrass meadows that are not excessively dense and characterize well-illuminated substrates.

From a paleoceanographic perspective, the presence of siliciclastic silt grains in both proximal and distal environments may indicate upwelling settings, regional current patterns, fluvial influx from hinterland, or dust supply. In this context, our ramp aligns with recent studies from highly productive warm-waters in transitional upwelling zones, such as the Mauritanian Golfe d'Arguin (Michel et al., 2011, 2019; Reymond et al., 2014; Klicpera et al., 2015) and the western Nicaragua Rise (Hine et al., 1987; Hallock, 1988; Hallock et al., 1988), where the high nutrient levels has been correlated with the suppression of carbonate production of LBF and z-corals.

5.3. Geodynamic and paleogeographic implications

The Eocene platforms examined were deposited in the southwestern part of the Atlas System, enclosed within the Casablanca-Azrou-Agadir triangle (Fig. 9) as indicated by Herbig (1991), Trappe (1992), Herbig and Trappe (1994), and Amelieh et al., 2026. It is generally accepted that the Bekrit-Timahdite Formation, part of the Sub-Atlas Group, dates from the Thanetian to Lutetian age. However, the Thanetian may be absent in certain sectors. Our biostratigraphic data on the Eocene Bekrit Timahdite Fm are very limited, and therefore the proposed age is also based on literature (Geyer and Herbig, 1988; Herbig, 1991, 1993; Granier et al., 1997, 2002; Scheibner and Speijer, 2008: Mebrouk et al., 2009; Dragastan et al., 2012; El Attmani et al., 2021; Amelieh et al.,

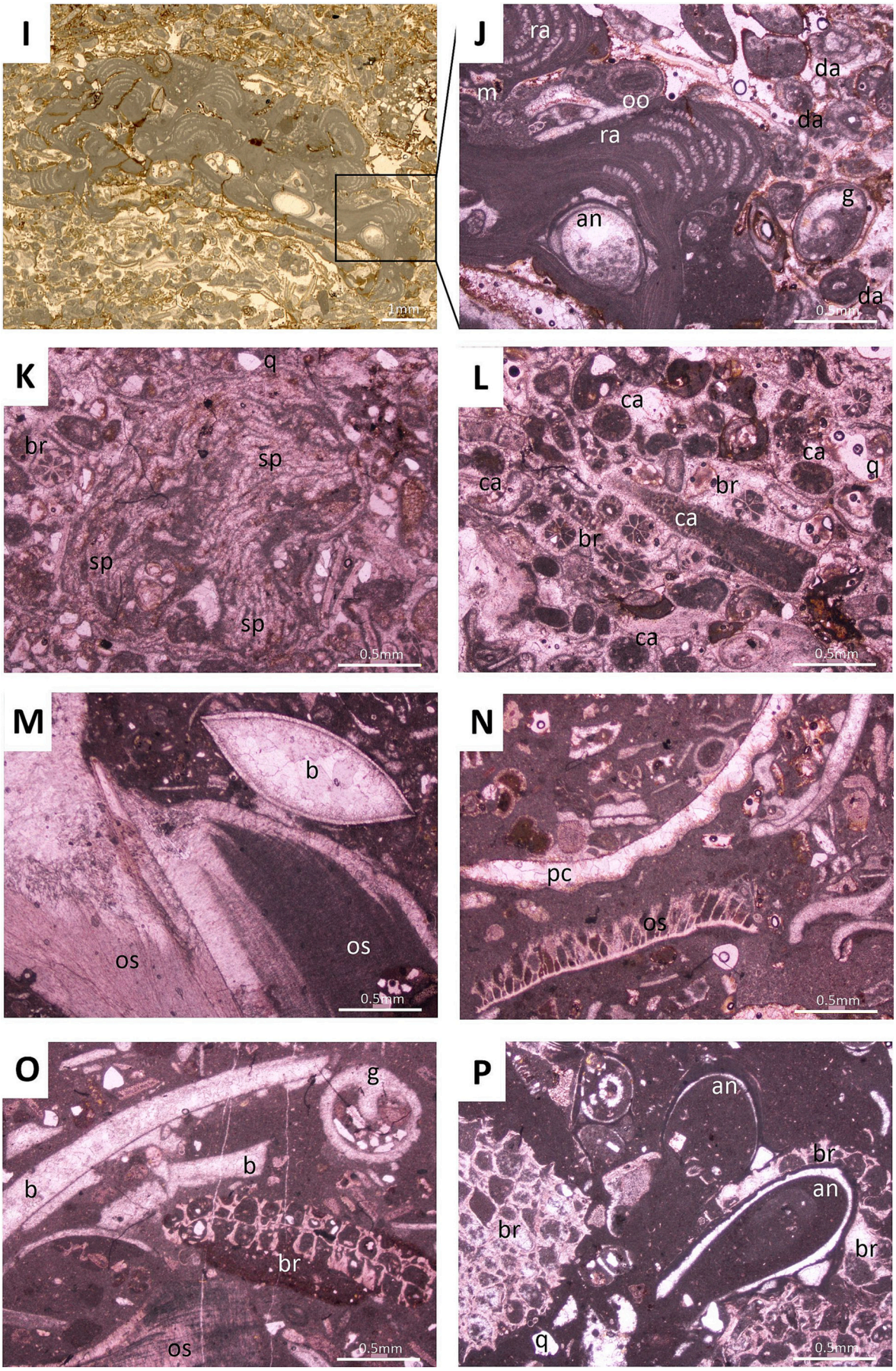

Fig. 7. (*continued*).

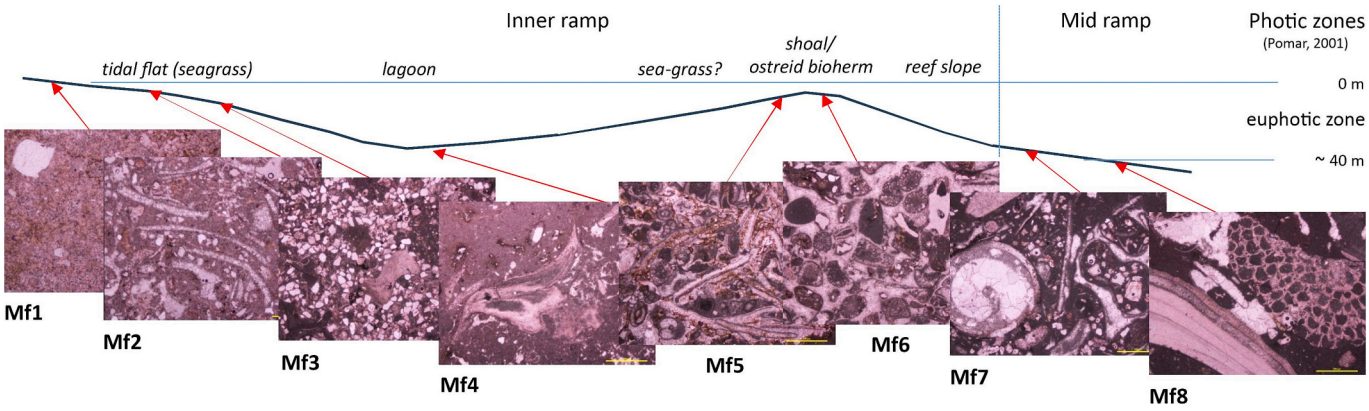

Fig. 8. Distribution of the environmental microfacies in the Eocene marine platforms of the Bekrit-Timahdite sector (Middle Atlas, Morocco): Mf1) Supratidal environment; Mf2) Intertidal-to-subtidal deposits, inner ramp environment; Mf3) Subtidal deposits, inner ramp environment; Mf4) Deep-lagoon deposits, inner ramp environment; Mf5) Reworked oyster bank at back-shoal, inner ramp environment; Mf6) Shoal deposits and ostreid bioherm (biostrome), inner ramp environment; Mf7) Open marine deposits, proximal mid ramp environment; Mf8) Open marine deposits, proximal mid ramp environment.

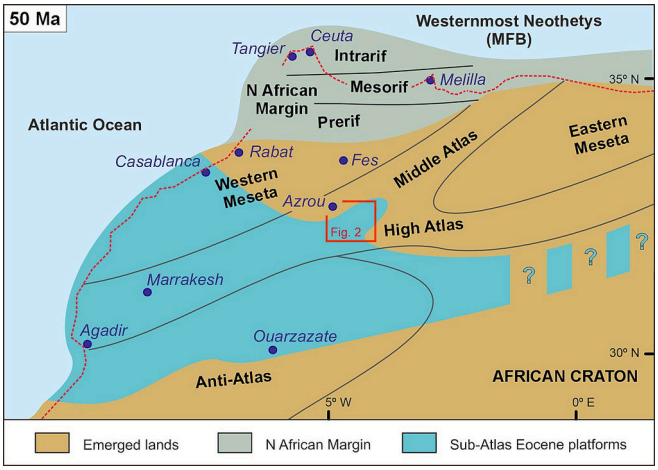

Fig. 9. Paleogeographic map of the Sub-Atlas Group during the Eocene, modified from Herbig (1991), Trappe (1992), Herbig and Trappe (1994), and Amelieh et al., 2026, highlighting the location of the study area (Fig. 2).

2026) assigning an Ypresian-Lutetian age to the Bekrit-Timahdite Formation, although this age remains poorly constrained. Folding events are expected from the Cretaceous-Tertiary (K-T) boundary on, in relation with the tectonic inversion occurring then across many peri-Neotethyan domains, likely driven by the acceleration of South Atlantic opening (Williams et al., 1989). The Thanetian is sometimes present in the synclines but absent in the anticlines, suggesting a syn-sedimentary tectonic activity during the Paleogene, in line with the Pyrenean tectonic phase (Martín-Martín et al., 2001). This tectonics has been referenced in several studies as a result of the Eo-Alpine compressive phase in the Neo-Tethys realms (Guerrera et al., 2006, 2014, 2021; Martín-Martín et al., 2023a, 2023b). The folding in key-areas, such as the Atlas Chain, likely resulted in a narrow depressed area (synclinorium) in the Saharian back zone, which had an Atlantic connection. Recently, similar Paleocene-Eocene facies, rich in phosphates and oyster reefs, have been documented in the eastern Saharian Zone, particularly in Algeria and Tunisia (Chadi et al., 2013; Kechiched et al., 2020; Boulemia and Adnet, 2023).

According to Duée et al. (1977) and Robbilard (1978, 1979), the Northern Middle Atlas Fault (NMAF) (Fig. 2) which runs between Logs 1–3 and Logs 4–5 is a strike-slip fault that remained active from the late Early Jurassic to the Oligocene. This fault had also a vertical component of motion, resulting in the formation of distinct shoals and basins. Herbig (1988) demonstrated the synsedimentary activity of the NMAF on the basis of facies differences between the Bekrit Syncline and Bou Anguer Syncline, situated on its opposed sides. As it is shown in Fig. 10, the thicknesses of the sedimentary successions (without compaction restoring) on the NMAF opposite sides are significantly different. Thus, Logs 4 and 5, belonging to the Folded Middle Atlas Block, are thicker than Logs 1 to 3 from Tabular Middle Atlas Block. As such, the Folded Middle Atlas Block must have been the subsident one during their sedimentation.

Fig. 10 illustrates the deduced rims of the ramp-like carbonate Eocene platform, drawing on data from litho- and microfacies. The innermost ramp (tidal flat) to mid ramp (reef slope) are depicted in various colors, with inner ramp sections (lagoon and bioherm-reefs) also represented. The upward stacking of these facies rims in each section have enabled us to deduce the sequence trends. In most cases, these sequences appear to be transgressive (T), with only two cases showing regressive trends (R). This result was anticipated, as shallow sedimentary realms typically experience emergence and erosion during regressions, leaving no trace in the sedimentary record. The deduced sequences can be defined as Low Frequency Sequences (Catuneanu, 2019; Haq and Ogg, 2024; Miclăuș et al., 2025), which correlate likely with 3rd-order cycles (1–10 Myr) caused by global sea-level changes and regional tectonics. In Logs 1 to 4, three T intervals are identified, while Log 5 displays only two T ones. Regressive intervals (R) occur at the base of Log 4 and at the end of the lower T interval in Log 2. Furthermore, rapid regressions (Ra.R) are constated when T intervals have no any regressive ones. Similarly, rapid transgressions (Ra.T) occur when T sequences show abrupt transitions from shallow to open environments, lacking certain ramp facies rims. In all cases, these sequences are believed to be influenced by regional tectonic pulses associated with the Eo-Alpine phase.

5.4. *Synthetic comparison with other nearby domains*

Recent studies on Paleocene-Eocene sedimentary successions and their paleogeographic models (Guerrera et al., 2021; Martín-Martín et al., 2020c, 2021, 2023a, 2025b, 2024, 2025a, 2025b, 2025c; Tosquella et al., 2022, 2025; Miclăuș et al., 2025) suggest the co-existence of several oceanic branches or basins in the western Tethys with their margins hosting belts of Paleocene-Eocene platforms rich in larger benthic foraminifera (LBF) and z-corals. In contrast, this study and others have documented the presence of carbonate platforms characterized by oysters, fish remainds, and phosphorites in the Middle Atlas and Saharan Zones from Morocco to Tunisia (Segonzac et al., 1986; Herbig, 1986, 1988, 1991, 1993; Herbig and Gregor, 1990; Trappe,

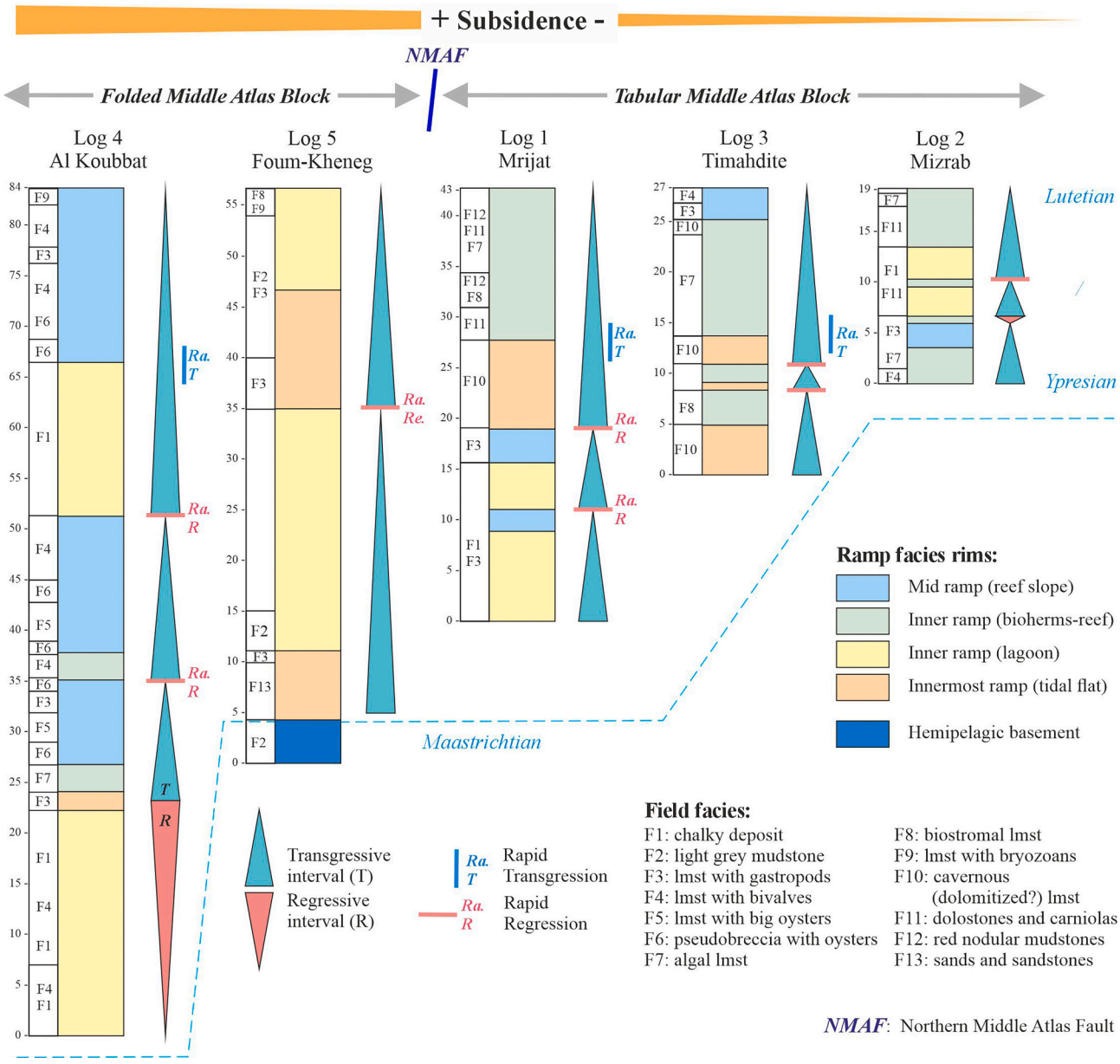

Fig. 10. Deduced sequences and trends in the Eocene studied sections located on the Folded Middle Atlas Block and the Tabular Middle Atlas Block, thickness analysis and subsidence proposals. The lateral variation of subsidence is given in the uppermost part of the figure. The defined field lithofacies (F1-F13) and the interpreted palaeoenvironments based on microfacies are also shown. Abbreviations: T – Transgressive interval (blue triangles); R – Regressive interval (red triangles); Ra.T – rapid transgression (short blue vertical line); Ra.R – rapid regression (short red horizontal line).

1991, 1992; Granier et al., 1997, 2002; Scheibner and Speijer, 2008; Chadi et al., 2013; Kechiched et al., 2020; Boulemia and Adnet, 2023). This section provides a comparison with the carbonate platforms of other adjacent sectors in the Neo-Tethys region. Fig. 11 presents a box with a paleogeographic sketch map for Eocene times, with the locations of the compared areas, as well as simplified Upper Cretaceus-Eocene stratigraphic columns from the Morocco to Tunisia, in north Africa, and from Spain to Italy, in Europe.

The Upper Cretaceous lithostratigraphic units, such as the Capas Blancas, Scaglia, or Abiod formations, often exhibit scaglia-like characteristics, primarily consisting of marly limestones and marls. Other facies may also occur, including: (1) phosphorite-bearing sands in the study area (El Koubbat Fm; 2 in Fig. 11) and the Algerian Saharan Domain (also 2 in Fig. 11); (2) massive caprinid limestones in the Pyrenean and Sicilian domains (5 and 7, respectively, in Fig. 11) and (3) radiolitid limestones in the Apenninic Domain (8 in Fig. 11). In all cases, these Upper Cretaceous deposits transitioned into a variety of shallow marine deposits in the Paleogene. This diversification may be linked to climatic changes, yet the significant influence of Eo-Alpine compressive tectonics should also be considered (Guerrera and Martín-Martín, 2014; Guerrera et al., 2021; Martín-Martín et al., 2025c). This initial phase of compressive tectonics is associated with the pre-foredeep stage, which involves basement folding (Fig. 11). In the study area (Bekrit-Timahdite Formation) and the Algerian Saharian Domain (Gafsa-Metlaoui Formation), deposits characterized by marshy (lagoonal) environments and limestone platforms rich in oysters, fish remains and phosphate levels have been recognized (1 and 2 in Fig. 11), and are also indicated by the published literature (Segonzac et al., 1986; Herbig, 1986, 1988, 1991, 1993; Herbig and Gregor, 1990; Trappe, 1991, 1992; Granier et al., 1997, 2002; Scheibner and Speijer, 2008; Chadi et al., 2013; Kechiched et al., 2020; Boulemia and Adnet, 2023). In the Prebetic Domain of the South Iberian Margin (3 in Fig. 11), three informal Paleocene-Eocene

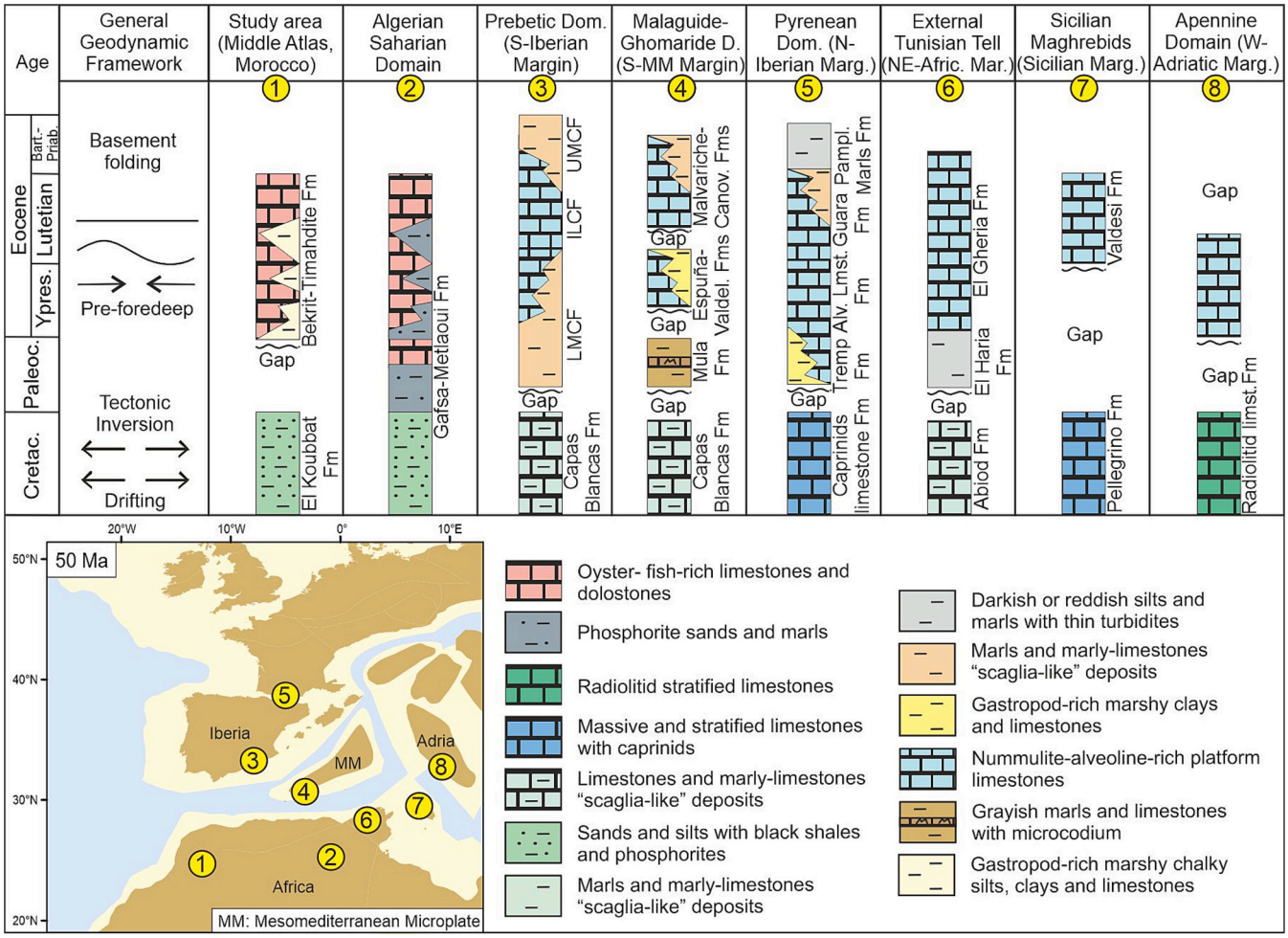

Fig. 11. Stratigraphic chart illustrating the correlation of the study area (1) with other adjacent sectors: (2) Algerian Saharian Domain; (3) Prebetic Domain from the South Iberian Margin (External Betic Zone: southearn Spain); (4) Malaguide-Ghomaride Domain from the south margin of the MM/Mesomediterranean Microplate (Internal Betic-Rif Zone: southern Spain and northern Morocco); (5) Pyrenean Domain from the North Iberian Margin (northeastern Spain); (6) Tunisian Tell Domain form the northeastern African Margin; (7) Sicilian Maghrebid Domain from the Sicilian Margin (southearn Italy); (8) Apennine Domain from the western Adriatic Margin (southearn Italy).

formations, rich in larger benthic foraminifera (LBF) and z-corals, have recently been defined (Martín-Martín et al., 2025c; and references therein). These formations, younging-up listed are: the Lower Marly-Clayey Formation (LMCF), the Intermediate Limestone-Calcarenite Formation (ILCF), and the Upper Marly-Clayey Formation (UMCF). They represent a transition from the inner to mid ramp (ILCF) and to the external ramp (LMCF and UMCF). A similar situation is observed in the Malaguide-Ghomaride Domain (4 in Fig. 11) situated on the Southern margin of the Mesomediterranean Microplate (MM), currently part of the Internal Zone of the Betic-Rif Cordilleras in southern Spain and northern Morocco. Numerous carbonate platform deposits from the Cuisian to Bartonian, rich in LBF and z-coral have been proposed, including the Mula, Espuña, Valdelaparra, Malvariche, and Cánovas formations, according to recent literature (Martín-Martín et al., 2020c, 2021, 2023a; Tosquella et al., 2022; Bullejos and Martín-Martín, 2025). In the Pyrenean Domain (5 in Fig. 11), the Paleocene-Eocene deposits comprise Paleocene "Garumnian facies", the lower-middle Eocene Tremp, *Alveolina*, Boltaña, and Guara limestone formations, along with the upper Eocene Pamplona Marl Formation. The Eocene formations mainly featuring LBF- and z-corals-rich limestones (Remacha et al., 1998; Martín-Martín et al., 2001; Barnolas et al., 2004; Gil-Peña et al., 2012; Pickering and Cantalejo, 2015; Roigé et al., 2016). In the External Tunisian Tell Domain from the Northeast African Margin (6 in Fig. 11), the El Haria and Gheria formations have been defined according to various studies (Van Houten, 1980; Wildi, 1983; Rouvier, 1985; Belayouni et al., 2010, 2012, 2023a, 2023b). They represent the transition from an inner-mid ramp (El Gheria) to external ramp (El Haria Formation).

The Sicilian Maghrebid Domain of the Sicilian Margin (7 in Fig. 11) contains similar deposits to the Tunisian Tell (Catalano et al., 2013; Chadi et al., 2013; Lentini and Carbone, 2014; Basilone, 2018; Basilone and Di Maggio, 2016; Benedetti, 2019; Henriquet et al., 2020; and references therein). The Valdesi Formation can be considered a lateral equivalent of the El Gheria Formation in the Panormide carbonate ramp, with both formations rich in LBF and z-corals. To conclude this comparison, the Apennine Domain from the Adriatic Margin (8 in Fig. 11) also shows carbonate platforms rich in LBF and z-corals, particularly in the Puglia area (southeastern, Italy) as mentioned by Vitale et al. (2018).

There is a notable homogeneity of limestone platforms rich in larger benthic foraminifera (LBF) and, to a lesser extent, z-corals across the Neo-Tethys platform belts extending from Spain to southern Italy. In contrast, the study area in the Middle Atlas and the correlated Algerian Saharan Domain lack such formations. In their cases, LBF and z-corals are replaced by limestones rich in oysters and fish remains, as well as phosphate levels, typical for nutrient-rich Atlantic-like upwelling zones. Although a connection with the Neo-Tethys has been proposed for the Algerian-Tunisian Domain (Kechiched et al., 2020; Boulemia and Adnet, 2023), we rather believe that its possible connection with Atlantic areas

is worth for future exploration. This connection may involve a narrow corridor from the Atlas-Mesetas System to Atlantic (Figs. 9 and 11), likely associated with basement folding during the Eo-Alpine tectonic phase, which would have created a synclinorium area within the uplifted Atlas-Mesetas ensemble as a horst or anticlinorium.

6. Conclusions

F1 to F13 field facies were distinguished based on lithology, sedimentary structures, and macrofossil content in five studied sections.

The biostratigraphic analysis using dinoflagellates, planktonic foraminifera, and calcareous nannoplankton yielded limited results. The top of the Cretaceous basement is Maastrichtian (not terminal). In contrast, the Paleogene succession is Lutetian suggesting a gap in sedimentation across the K/T boundary.

A microfacies study was conducted, which enabled the identification of eight microfacies (Mf1 to Mf8), each representing different facies rims of a ramp-like carbonate platform: the inner ramp (Mf1 to Mf6, including supratidal, lagoon, shoals, oyster-rich reef bioherm) and the mid ramp (Mf7 and Mf8, representing reef slope and open marine environments).

The recognized mixture of Eocene photozoan and heterotrophic organisms indicates thriving marine conditions within meso- to eutrophic waters.

Three carbonate factories are defined: tropical heterozoan warm-water factory on inner ramp; bryozoan-molluscan dominated carbonate factory on the innermost mid ramp; and rhodalgal factory in the mid ramp. Their development conditions correlate with the 'photozoan factory', highlighting the 'photozoan-to-heterozoan transition', showing partial similarities with the 'C-factory'.

The studied Eocene platforms were developed in the southwestern region of the Atlas-Mesetas System coeval with the opening of the South Atlantic and the Pyrenean Eo-Alpine tectonic phase where the folding of the Atlas Chain likely resulted in a narrow, depressed hinterland area that maintained a connection with the Atlantic.

The Northern Middle Atlas Fault, which lies between the Folded and the Tabular Middle Atlas, allowed a higher subsidence in the first one, as the greater thickness of its sedimentary record shows.

The analyzed sedimentary deposits are organized into low frequency (likely 3rd-order) predominantly transgressive sequences (T) resulting from global sea-level fluctuations and regional tectonics linked to the Eo-Alpine phase. Rapid regressions (Ra.R) and transgressions (Ra.T) have also been identified.

A synthetic comparison with Cretaceous-Eocene successions from nearby sectors in the Neo-Tethys region reveals a notable homogeneity of ramp-like platforms rich in larger benthic foraminifera (LBF) and z-corals, extending from Spain to southern Italy. In contrast, the study area shows abundant oyster and fish remains, as well as phosphate levels, typical of nutrient-rich Atlantic up-welling zones. Similar features are known in Algerian Saharian Domain.

Although a connection with the Neo-Tethys has been suggested for the Algerian-Tunisian Domain, we believe that a link to Atlantic areas is likely, further exploration being necessary. This connection may involve a narrow corridor extending from the Atlas-Mesetas System to Atlantic during the Paleocene-Eocene period which could also explain the absence of LBF and z-corals.

CRediT authorship contribution statement

Manuel Martín-Martín: Writing – original draft, Supervision, Project administration, Investigation, Funding acquisition, Data curation, Conceptualization. **Josep Tosquella:** Writing – original draft, Methodology, Investigation. **Crina Miclăuș:** Writing – original draft, Investigation. **Ali Maaté:** Investigation. **José Enrique Tent-Manclús:** Investigation. **Soufian Maaté:** Investigation. **Eric Monteil:** Methodology, Investigation. **Francisco Serrano:** Methodology, Investigation. **José Antonio Martín-Pérez:** Investigation.

Declaration of competing interest

The authors declare that they have no known competing financial interests or personal relationships that could have appeared to influence the work reported in this paper.

Acknowledgements

This research was supported by the Spanish Ministry of Science and Innovation (Research Project PID2020-114381GB-I00) and by the Research Groups and Projects led by M. Martín-Martín at Alicante University (CTMA-IGA). The revisions performed by Prof. Giovanni Coletti and an anonymous reviewer are gratefully acknowledged.

Data availability

Data will be made available on request.

References

Abd El-Moghny, M.W., Afifi, A.A., 2022. Microfacies analysis and depositional environments of the Middle Eocene (Bartonian) Qurn Formation along Qattamiya-Ain Sokhna district. Egypt. Carbonates and Evaporites 37, 18. https://doi.org/10.1007/s13146-022-00762-9.

Abdelhady, A.A., Kassabb, W., Mohamed, F.A., 2019. Shoal environment as a biodiversity hotspot: A case from the Barremian Albian strata of Gabal Lagama (North Sinai, Egypt). Journal of African Earth Sciences 160, 103643. https://doi.org/10.1016/j.jafrearsci.2019.103643.

Aguirre, J., Riding, R., Braga, J.C., 2000. Diversity of coralline red algae: origination and extinction patterns from the early cretaceous to the Pleistocene. Paleobiology 26, 651–667.

Amelieh, A., Oukassou, M., Guinot, G., Zafaty, O., Mhamdi, H., Yans, J., Charrière, A., Tabuce, R., 2026. Biostratigraphy, palaeoenvironments and palaeogeography of the Cretaceous–Paleogene succession in the Oudiksou basin, Central Middle Atlas of Morocco. Palaeogeography, Palaeoclimatology, Palaeoecology 683, 113451. https://doi.org/10.1016/j.palaeo.2025.113451.

Amrani, S., 2016. Hydrodynamisme, hydrogéochimie et vulnérabilité de la nappe d'eau superficielle et leur relation avec la tectonique cassante dans la zone effondrée Timahdite – Almis Guigou (Moyen Atlas, Maroc) (Ph.D. thesis). Université Sidi Mohamed Ben Abdellah de Fès (Maroc), pp. 163 (in French).

Baccelle, L., Bosellini, A., 1965. Diagrammi per la stima visiva della composizione percentuale nelle rocce sedimentarie. Annali dell'Università di Ferrara, Nuova Serie, Sezione IX, Scienze geologiche e paleontologiche 1, 59–89 (in Italian).

Baceta, J.I., Mateu-Vicens, G., 2022. Seagrass development in terrigenous-influenced inner ramp settings during the middle Eocene (Urbasa–Andia Plateau, Western Pyrenees, North Spain). Sedimentology 69 (1), 301–344. https://doi.org/10.1111/sed.12937.

Barbosa, M., Lefler, F., Berthold, D.E., Dail Laughinghouse, H., 2021. The ecology of charophyte algae (Charales). EDIS 2021 (1). https://doi.org/10.32473/edis-ag448-2021. SS-AGR-448/AG448.

Barnolas, A., Payros, A., Samsó, J.M., Serra-Kiel, J., Tosquella, J., 2004. La Cuenca surpirenaica desde el Ilerdiense medio al Priaboniense. In: Vera, J.A. (Ed.), Geología de España. Sociedad Geológica de España – Instituto Geológico y Minero de España, Madrid, pp. 313–320 in Spanish.

Basilone, L., 2018. Lithostratigraphy of Sicily. In: UNIPA Springer Series. Springer, Cham, p. 349. https://doi.org/10.1007/978-3-319-73942-7.

Basilone, L., Di Maggio, C., 2016. Geology of Monte Gallo (Palermo Mts, NW Sicily). Journal of Maps 12 (5), 1072–1083. https://doi.org/10.1080/17445647.2015.1124716.

Belayouni, H., Brunelli, D., Clochiatti, R., Di Staso, A., El Amrani El Hassani, I.-E., Guerrera, F., Kasaa, S., Nejia, L.O., Martín-Martín, M., Serrano, F., Tramontana, M., 2010. La Galite Archipelago (Tunisia, North Africa): Stratigraphic and petrographic revision and insights for geodynamic evolution of the Maghrebian Chain. Journal of African Earth Sciences 56 (1), 15–28. https://doi.org/10.1016/j.jafrearsci.2009.05.004.

Belayouni, H., Guerrera, F., Martín-Martín, M., Serrano, F., 2012. Stratigraphic update of the Cenozoic Sub-Numidian formations of the Tunisian tell (North Africa): Tectonic/sedimentary evolution and correlations along the Maghrebian Chain. Journal of African Earth Sciences 64, 48–64. https://doi.org/10.1016/j.jafrearsci.2011.11.010.

Belayouni, H., Guerrera, F., Martin-Martin, M., Le Breton, E., Tramontana, M., 2023a. The Numidian formation and its lateral successions (Central-Western Mediterranean): A review. International Geology Review 65 (22), 3570–3602. https://doi.org/10.1080/00206814.2023.2199429.

Belayouni, H., Guerrera, F., Martín-Martín, M., Tramontana, M., Bullejos, M., 2023b. Cenozoic tectono-sedimentary evolution of the onshore-offshore Tunisian tell: Implications for oil-gas research. Marine and Petroleum Geology 156, 106426. https://doi.org/10.1016/j.marpetgeo.2023.106426.

Benamrane, M., Németh, K., Jadid, M., Talbi, E.H., 2022. Geomorphological Classification of Monogenetic Volcanoes and its Implication to Tectonic stress Orientation in the Middle Atlas Volcanic Field (Morocco). Land 11, 1893. https://doi.org/10.3390/land11111893.

Benedetti, A., 2019. Benthic foraminiferal assemblages from the late Eocene to the early Oligocene of the Caltavuturo Formation in the Madonie Mountains (Sicily): a tool for correlation. Italian Journal of Geosciences 138, 43–55. https://doi.org/10.3301/IJG.2018.25.

Bialik, O.M., Coletti, G., Mariani, L., Commissario, L., Desbiolles, F., Meroni, A.N., 2023. Availability and type of energy regulate the global distribution of neritic carbonates. Scientific Reports 13 (1), 19687. https://doi.org/10.1038/s41598-023-47029-4.

Boulemia, S., Adnet, S., 2023. A new Palaeogene elasmobranch fauna (Tebessa region, eastern Algeria) and the importance of Algerian-Tunisian phosphates for the North African fossil record. Annales de Paleontologie 109 (3), 102632. https://doi.org/10.1016/j.annpal.2023.102632.

Brandano, M., Tomassetti, L., Mateu-Vicens, G., Gaglianone, G., 2019. The seagrass skeletal assemblage from modern to fossil and from tropical to temperate: insight from Maldivian and Mediterranean examples. Sedimentology 66 (6), 2268–2296. https://doi.org/10.1111/sed.12589.

Bullejos, M., Martín-Martín, M., 2025. 3D modeling and visualization of geological structures with python-implemented Bézier curves/surfaces. Journal of Structural Geology 200, 105508. https://doi.org/10.1016/j.jsg.2025.105508.

Burchette, T.P., Wright, V.P., 1992. Carbonate ramp depositional systems. Sedimentary Geology 79, 3–57. https://doi.org/10.1016/0037-0738(92)90003-A.

Burollet, P.F., 1981. The Pelagian Sea east of Tunisia: bioclastic deposition under temperate climate. Marine Geology 44 (1–2), 157–170. https://doi.org/10.1016/0025-3227(81)90116-X.

Buxton, M.W.N., Pedley, H.M., 1989. Short Paper: a standardized model for Tethyan Tertiary carbonate ramps. Journal of the Geological Society 146 (5), 746–748. https://doi.org/10.1144/gsjgs.146.5.0746.

Catalano, R., Avellone, G., Basilone, A., Contino, A., Agate, M., 2013. Note illustrative della carta geologica d'Italia alla scala 1:50.000 Foglio 595 Palermo. In: Progetto CARG. ISPRA - Servizio Geologico d'Italia, p. 218. Roma. (in Italian). 10.15161/oar.it/143255.

Catuneanu, O., 2019. Scale in sequence stratigraphy. Marine and Petroleum Geology 106, 128–159. https://doi.org/10.1016/j.marpetgeo.2019.04.026.

Chadi, M., Brahim, E.H.Y., Djeffal, R., 2013. The southern Tellian series at nummulites (NE Algeria): stratigraphy and structural consequences. Conference Proceedings of the 1st Annual International Interdisciplinary Conference. AIIC 2013, 24-26 April 2013, Azores, Portugal. European Scientific Journal 9 (21), 460–466. http://eujournal.org/files/journals/1/books/aiic.vol.3.pdf.

Chafai, K., Hssaida, T., Maatouf, W., Slimani, H., Rjimati, E.-C., Afenzar, A., Louaya, A., Jaydawi, S., Chakir, S., Khaffou, H., 2024. Palynostratigraphy and paleoenvironment of upper cretaceous sedimentary deposits from the Tarfaya-Laayoune-Boujdour-Dakhla Basin, southwestern Morocco. Review of Palaeobotany and Palynology 327, 1–31. https://doi.org/10.1016/j.revpalbo.2024.105141.

Chakir, S., Slimani, H., Hssaida, T., Kocsis, L., Gheerbrant, E., Bardet, N., Jalil, N.-E., Mouflih, M., Mahboub, I., Jbari, H., 2020. Dinoflagellate cyst evidence for the age, palaeoenvironment and paleoclimate of a new Cretaceous-Paleogene (K/Pg) boundary section at the Bou Angueur syncline, Middle Atlas, Morocco. Cretaceous Research 106, 104219. https://doi.org/10.1016/j.cretres.2019.104219.

Chan, S.A., Kaminskia, M.A., Al-Ramadana, K., Babalolaba, L.O., 2017. Foraminiferal biofacies and depositional environments of the Burdigalian mixed carbonate and siliciclastic Dam Formation, Al-Lidam area, Eastern Province of Saudi Arabia. Palaeogeography, Palaeoclimatolology, Palaeoecology 469, 122–137. https://doi.org/10.1016/j.palaeo.2016.12.041.

Charrière, A., 1990. Héritage hercynien et évolution géodynamique alpine d'une chaine intracontinentale: le Moyen-Atlas au SE de Fès (Maroc) (Ph.D. thesis). Université Paul Sabatier, Toulouse III (Sciences), Toulouse, France, p. 589 (in French).

Choubert, G., Marcais, J., 1956. Introduction au Lexique stratigraphique du Maroc. Les grands traits de la géologie du Maroc. In: Choubert, G., Faure-Muret, A. (Eds.), Lexique stratigraphique du Maroc, Notes et Mémoires du Service Géologique du Maroc, 134, pp. 5–38 (in French).

Coletti, G., Basso, D., 2020. Coralline algae as depth indicators in the Miocene carbonates of the Eratosthenes Seamount (ODP Leg 160, Hole 966F). Geobios 60, 29–46. https://doi.org/10.1016/j.geobios.2020.03.005.

Coletti, G., Commissario, L., Mariani, L., Bosio, G., Desbiolles, F., Soldi, M., Bialik, O.M., 2022. Palaeocene to Miocene southern Tethyan carbonate factories: a meta-analysis of the successions of South-western and Western Central Asia. The Depositional Record 8 (3), 1031–1054. https://doi.org/10.1002/dep2.204.

Colo, G., 1961. Contribution à l'étude du jurassique du Moyen-Atlas septentrional. Notes et Mémoires du Service Géologique du Maroc 139, 226 (in French).

Dragastan, O.N., Herbig, H.G., 2007. *Halimeda* (green siphonous algae) from the Paleogene of (Morocco) – Taxonomy, phylogeny and paleoenvironment. Micropaleontology 53 (1–2), 1–72. https://doi.org/10.2113/gsmicropal.53.1-2.1.

Dragastan, O.N., Herbig, H.G., Popa, M.E., 2012. Paleogene Halimeda algal biostratigraphy from Middle Atlas and Central High Atlas (Morocco), paleoecology, paleogeography and some taxonomical considerations. Acta Palaeontologica Romaniae 8 (1–2), 43–90.

Duée, G., Hervouet, Y., Laville, E., De Lucas, P., Robillard, D., 1977. L'accident nord moyen-atlasique dans la région de Boulemane (Maroc): une zone de coulissement synsédimentaire. In: Annales De La Société Géologique Du Nord, 98-2, pp. 45–162. French. https://www.persee.fr/doc/asgn_0767-7367_1978_num_98_2_1355.

Ekin, I., 2024. Paleoenvironmental insights from the early Miocene oysters in the shallow-marine deposits of the Fırat formation in Diyarbakır. SE Turkey. Annales de Paléontologie 110 (2), 102660. https://doi.org/10.1016/j.annpal.2023.102660.

El Attmani, M., Bouwafoud, A., Elouariti, S., Si Mhamdi, H., Ben Bouziane, A., Mouflih, M., 2021. Late Cretaceous-Paleogene Formation of the Bekrit Syncline, Middle Atlas, Morocco: Sedimentology, Geochemistry, Palinology and Paleonvironments. Open Journal of Geology 11, 61–80. https://doi.org/10.4236/ojg.2021.113005.

El-Omla, M.M., Aboulela, H.A., 2012. Environmental and Mineralogical Studies of the Sabkhas Soil at Ismailia—Suez Roadbed, Southern of Suez Canal District. Egypt. Open Journal of Geology 2 (3), 165–181. https://doi.org/10.4236/ojg.2012.23017.

Embry, A.F., Klovan, J.E., 1971. A late Devonian reef tract on northeastern Banks Island, NWT. Bulletin of Canadian Petroleum Geology 19 (4), 730–781. https://doi.org/10.35767/gscpgbull.19.4.730.

Fedan, B., 1988. Evolution géodynamique d'un bassin intraplaque sur décrouchements: le Moyen-Atlas (Maroc) durant le Méso-Cénozoïque (Ph.D. thesis). Université Mohammed V, Rabat, Maroc, pp. 338 (in French).

Fensome, R.A., MacRae, R.A., Williams, G.L., Fauconnier, C., Grothe, A., Hopkins, A.M., Ikävalko, E., Riding, J.B., Skupien, P., de Verteuil, L., Williams, G., 2019. Index of Fossil Dinoflagellates 2019, 50. American Association of Stratigraphic Palynologists, Contributions Series.

Fernández-Landero, S., Fernández-Caliani, J.C., 2021. Mineralogical and Crystal-Chemical Constraints on the Glauconite-Forming Process in Neogene Sediments of the lower Guadalquivir Basin (SW Spain). Minerals 11, 578. https://doi.org/10.3390/min11060578.

Flores, J.A., Sierro, F.J., 1997. Revised technique for calculation of calcareous nannofossil accumulation rates. Micropaleontology 43 (3), 321–324.

Flügel, E., 2010. Microfacies of Carbonate Rocks. Analysis, Interpretation and Application. Springer Berlin, Heidelberg, p. 976.

Geyer, G., Herbig, H.G., 1988. New Eocene oysters and the final regression at the southern rim of central High Atlas (Morocco). Geobios 21 (6), 663–684. https://doi.org/10.1016/S0016-6995(88)80087-1.

Gil-Peña, I., Barnolas, A., Montes Santiago, M., García Ruiz, J.M., Peña Monné, J.L., Martí Bono, C., Gómez Villar, A., 2012. Hoja geológica y memoria n° 177 (Sabiñánigo). Mapa Geológico de España 1:50.000, 2ª ser. (MAGNA), I.G.M.E, p. 82. In Spanish.

Granier, B., 2012. The contribution of calcareous green algae to the production of limestones: a review. Geodiversitas 34 (1), 35–60. https://doi.org/10.5252/g2012n1a3.

Granier, B., M.A., Ait Sliman, Fedan, B., 1997. Triploporella? atlasica n.sp., une Dasycladacée (algue verte) du Palócène-Eocène de l'Atlas moyen Maroc. Revue de Paléobiologie 16 (1), 47–53. Genève. (in French).

Granier, B., Ait Sliman M.A., Fedan, B., 2002. Validation de l'espèce Triploporella atlasica Granier, Ait Sliman et Fedan, non 1997. In: Bucur, I.I., Filipescu, S. (Eds.), Research Advances in Calcareous Algae and Microbial Carbonates. Proceedings of the 4th IFAA Regional Meeting, August 29 – September 5 2001, Cluj-Napoca. Cluj University Press, Romania, pp. 115–116 (in French).

Guédé, K.E., Slimani H Guédé, K.E., Slimani, H., Louwye, S., Asebriy, L., Toufiq, A., Ahmamou, M.F., El Amrani El Hassani, I.E., Digbehi, Z.B., 2014. Organic-walled dinoflagellate cysts from the Upper Cretaceous–lower Paleocene succession in the western External Rif, Morocco: new species and new biostratigraphic results. Geobios 47 (5), 291–304. https://doi.org/10.1016/j.geobios.2014.06.006.

Guerrera, F., Martín-Martín, M., 2014. Geodynamic events reconstructed in the Betic, Maghrebian, and Apennine chains (central-western Tethys). Bulletin de la Société Géologique de France 185 (5), 329–341. https://doi.org/10.2113/gssgfbull.185.5.329.

Guerrera, F., Estévez, A., López-Arcos, M., Martín-Martín, M., Martín-Pérez, J.A., Serrano, F., 2006. Paleogene tectono-sedimentary evolution of the Alicante trough (external Betic zone, SE Spain) and its bearing on the timing of the deformation of the south Iberian margin. Geodinamica Acta 19 (2), 87–101. https://doi.org/10.3166/ga.19.87-101.

Guerrera, F., Mancheño, M.A., Martín-Martín, M., Raffaelli, G., Rodríguez-Estrella, T., Serrano, F., 2014. Paleogene evolution of the External Betic Zone and geodynamic implications. Geologica Acta 12 (3), 171–192. https://doi.org/10.1344/GeologicaActa2014.12.3.1.

Guerrera, F., Martín-Martín, M., Tramontana, M., 2021. Evolutionary geological models of the central-western peri-Mediterranean chains: a review. International Geology Review 63 (1), 65–86. https://doi.org/10.1080/00206814.2019.1706056.

Hallock, P., 1988. The role of nutrient availability in bioerosion: consequences to carbonate buildups. Palaeogeography, Palaeoclimatology, Palaeoecology 63 (1–3), 275–291. https://doi.org/10.1016/0031-0182(88)90100-9.

Hallock, P., Glenn, E.C., 1986. Larger foraminifera: a tool for paleoenvironmental analysis of Cenozoic carbonate depositional facies. Palaios 1 (1), 55–64. https://doi.org/10.2307/3514459.

Hallock, P., Schlager, W., 1986. Nutrient excess and the demise of coralreefs and carbonate platforms. Palaios 1 (4), 389–398. https://doi.org/10.2307/3514476.

Hallock, P., Hine, A.C., Vargo, G.A., Elrod, J.A., Jaap, W.C., 1988. Platforms of the Nicaraguan rise: examples of the sensitivity of carbonate sedimentation to excess trophic resources. Geology 16 (12), 1104–1107. https://doi.org/10.1130/0091-7613(1988)016%3C1104:POTNRE%3E2.3.CO;2.

Hansen, J.M., 1977. Dinoflagellate stratigraphy and echinoid distribution in Upper Maastrichtian and Danian deposits from Denmark. Bulletin of the Geological Society of Denmark 26, 1–26. https://doi.org/10.37570/bgsd-1976-26-01.

Hansen, J.M., 1979. A new dinoflagellate zone at the Maastrichtian/Danian boundary in Denmark. Danmarks Geologiske Undersøgelse Årbog 1979, 131–140.

Haq, B.U., Ogg, J., 2024. Retraversing the highs and lows of Cenozoic sea levels. GSA Today 34 (6), 4–11. https://doi.org/10.1130/GSATGG593A.1.

Hennissen, J.A.I., Wood, S.E.L., Flint, J., 2018. The Standard Palynological Preparation Protocol used in the Biostratigraphy and Palaeontology Laboratories at the British Geological Survey. British Geological Survey Internal Report IR/18/43, pp. 18.
Henriquet, M., Dominguez, S., Barreca, G., Malavieille, J., Monaco, C., 2020. Structural and tectono-stratigraphic review of the Sicilian orogen and new insights from analogue modeling. Earth-Science Reviews 208, 103257. https://doi.org/10.1016/j.earscirev.2020.103257.
Herbig, H.G., 1986. Lithostratigraphisch-fazielle Untersuchungen im marinen Alttertiär südlich des zentralen Hohen Atlas (Marokko). Berliner geowisschaftliche Abhandlungen (A) 66, 343–380 (in German with English Abstract).
Herbig, H.G., 1988. Synsedimentary tectonics in the Northen Middle Atlas (Morocco) during the late cretaceous and tertiary. In: Jacobshagen, V.H. (Ed.), The Atlas System of Morocco, Lecture Notes in Earth Sciences, 15. Springer, Berlin, Heidelberg, pp. 321–338. https://doi.org/10.1007/BFb0011599.
Herbig, H.G., 1991. Das Paläogen am Südrand des zentralen Hohen Atlas und im Mittleren Atlas Marokkos. Stratigraphie, Fazies, Paläogeographie und Paläotektonic, 135. Berliner geowisschaftliche Abhandlungen (A), p. 289 in German with English Abstract.
Herbig, H.G., 1993. Stratigraphy, facies and synsedimentry tectonics of the post-Middle Eocene Tertiary, Middle Atlas West of Boulemane (Morocco). Neues Jarhbuch für Geologie und Paläontologie - Abhandlungen 188, 1–50. https://doi.org/10.1127/njgpa/188/1993/1.
Herbig, H.G., Fechner, G.G., 1994. Cretaceous and early tertiary stratigraphy, fades and palynology of the eastern Bou Angueur syncline, Middle Atlas Mountains, Morocco. Zeitschrift der Deutschen Geologischen Gesellschaft 145 (2), 249–273.
Herbig, H.G., Gregor, H.J., 1990. The mangrove-forming palm *Nypa* from the early Paleogene of southern Morocco. Paleoenvironment and paleoclimate. Géologie Méditerranéenne 27 (2), 123–137.
Herbig, H.G., Trappe, J., 1994. Stratigraphy of the Subatlas Group (Maastrichtian-Middle Eocene). Morocco. Newsletter on Stratigraphy 30 (3), 125–165. https://doi.org/10.1127/nos/30/1994/125.
Hinaje, S., 2004. Tectonique cassante et paléochamps de contraintes dans le moyen atlas et le haut atlas central (Midelt-Errachidia) depuis le trias jusqu'à l'actuel (Ph.D thesis). Université Mohammed V, Rabat, Maroc, p. 363 (in French).
Hine, A.C., Hallock, P., Harris, M.W., Mullins, H.T., Belknap, D.F., Jaap, W.C., 1987. Halimeda Bioherms along an open seaway: Miskito Channel, Nicaraguan rise, SW Caribbean Sea. Coral Reefs 6, 173–178. https://doi.org/10.1007/BF00302013.
Jbari, H., Slimani, H., 2022. Paleoenvironmental and paleoclimatic changes during the late Cretaceous and Cretaceous–Paleogene (K/Pg) boundary transition in Tattofte, External Rif, northwestern Morocco: implications from dinoflagellate cysts and palynofacies. Palaeoworld 31, 334–357. https://doi.org/10.1016/j.palwor.2021.08.002.
Jbari, H., Slimani, H., Chekar, M., Asebriy, L., Benzaggagh, M., Mahboub, I., Chakir, S., 2020. Campanian to Danian dinoflagellate cyst assemblages from the southwestern Tethyan margin (Tattofte section, western External Rif, Morocco): Biostratigraphic and paleobiogeographic interpretations. Review of Palaeobotany and Palynology 279, 104225. https://doi.org/10.1016/j.revpalbo.2020.104225.
Kassab, W., Santos, A., El Hedeny, M., Al Farraj, S., Al Basher, G., Rashwan, M., 2021. Late Eocene marginal marine deposits and paleoenvironment characterisation from the Maadi Formation (Northern Eastern Egypt). Proceedings of the Geologists' Association 132 (3), 346–357. https://doi.org/10.1016/j.pgeola.2021.02.003.
Kechiched, R., Laouar, R., Bruguier, O., Kocsis, L., Salmi-Laouar, S., Bosch, D., Ameur-Zaimeche, O., Foufou, A., Larit, H., 2020. Comprehensive REE+Y and sensitive redox trace elements of Algerian phosphorites (Tébessa, eastern Algeria): A geochemical study and depositional environments tracking. Journal of Geochemical Exploration 208, 106396. https://doi.org/10.1016/j.gexplo.2019.106396.
Kennett, J.P., Stott, L.D., 1991. Abrupt deep-sea warming, palaeoceanographic changes and benthic exitnctions at the end of the Palaeocene. Nature 353, 225–229. https://doi.org/10.1038/353225a0.
Klicpera, A., Michel, J., Westphal, H., 2015. Facies patterns of a tropical heterozoan carbonate platform under eutrophic conditions: the Banc d'Arguin, Mauritania. Facies 61, 421. https://doi.org/10.1007/s10347-014-0421-5.
Lentini, F., Carbone, S., 2014. Geologia della Sicilia (geology of Sicily). Memorie Descrittive della Carta Geologica d'Italia 95, 7–414 (in Italian with English abstract).
Lorenz, J.C., 1976. Triassic sediments and basin structure of the Kerrouchen basin, central Morrocco. Journal of Sedimentary Research 46 (4), 897–905. https://doi.org/10.1306/212F7086-2B24-11D7-8648000102C1865D.
Martini, E., 1971. Standard Tertiary and Quaternary calcareous nannoplankton zonation. In: Farinacci, A. (Ed.), Proceedings of the 2nd Planktonic Conference, Rome 1970. Tecnoscienza, Roma, Italy, pp. 739–785.
Martín-Martín, M., Rey, J., Alcala-Garcia, F.J., Tosquella, J., Deramond, J., Lara-Corona, E., Duranthon, F., Antoine, P.O., 2001. Tectonic controls on the deposits of a foreland basin: an example from the Eocene Corbieres-Minervois basin, France. Basin Research 13 (4), 419–433. https://doi.org/10.1046/j.0950-091x.2001.00158.x.
Martín-Martín, M., Guerrera, F., Tosquella, J., Tramontana, M., 2020a. Paleocene-lower Eocene carbonate platforms of westernmost Tethys. Sedimentary Geology 404, 105674. https://doi.org/10.1016/j.sedgeo.2020.105674.
Martín-Martín, M., Guerrera, F., Tramontana, M., 2020b. Geodynamic implications of the latest Chattian-Langhian central-western peri-Mediterranean volcano-sedimentary event: a review. The Journal of Geology 128 (1), 29–43. https://doi.org/10.1086/706262.
Martín-Martín, M., Guerrera, F., Miclăuș, C., Tramontana, M., 2020c. Similar Oligo-Miocene tectono-sedimentary evolution of the Paratethyan branches represented by the Moldavidian Basin and Maghrebian Flysch Basin. Sedimentary Geology 396, 105548. https://doi.org/10.1016/j.sedgeo.2019.105548.
Martín-Martín, M., Guerrera, F., Tosquella, J., Tramontana, M., 2021. Middle Eocene carbonate platforms of the westernmost Tethys. Sedimentary Geology 415, 105861. https://doi.org/10.1016/j.sedgeo.2021.105861.
Martín-Martín, M., Perri, F., Critelli, S., 2023a. Cenozoic detrital suites from the Internal Betic-Rif Cordilleras (S Spain and N Morocco): implications for paleogeography and paleotectonics. Earth-Science Reviews 243, 104498. https://doi.org/10.1016/j.earscirev.2023.104498.
Martín-Martín, M., Tosquella, J., Guerrera, F., Maaté, A., Hlila, R., Maaté, S., Tramontana, M., Le Breton, E., 2023b. The Eocene carbonate platforms of the Ghomaride Domain (Internal Rif Zone, N Morocco): A segment of the westernmost Tethys. Sedimentary Geology 452, 106423. https://doi.org/10.1016/j.sedgeo.2023.106423.
Martín-Martín, M., Guerrera, F., Cañaveras, J.C., Alcalá, F.J., Serrano, F., Maaté, A., Hlila, R., Maaté, S., Sánchez-Navas, A., Miclăus, C., Tent-Manclús, J.E., Bullejos, M., 2024. Miocene evolution of the External Rif Zone (Morocco): Comparison with similar and lateral southern Mediterranean Tethyan margins. Sedimentary Geology 464, 106619. https://doi.org/10.1016/j.sedgeo.2024.106619.
Martín-Martín, M., Tosquella, J., Guerrera, F., Maaté, A., Martín-Algarra, A., 2025a. The eocene carbonate platforms of the westernmost Tethys: a review. International Geology Review 1–33. https://doi.org/10.1080/00206814.2024.2397804.
Martín-Martín, M., Guerrera, F., Talmat, S., 2025b. Deciphering Paleogene platforms from a "lost domain" in the western Neo-Tethys. Earth Science Reviews 266, 105152. https://doi.org/10.1016/j.earscirev.2025.105152.
Martín-Martín, M., Miclăuș, C., Tent-Manclús, J.E., Tosquella, J., Serrano, F., Samsó, J. M., Martín-Pérez, J.A., 2025c. Paleocene-Eocene evolution of the Prebetics (south Iberian margin, South Spain) and comparison with other western Tethyan margins. Marine and Petroleum Geology 176, 107300. https://doi.org/10.1016/j.marpetgeo.2025.107300.
Mateu-Vicens, G., Brandano, M., Gaglianone, G., Baldassarre, A., 2012. Seagrass-meadow sedimentary facies in a mixed siliciclastic-carbonate temperate system in the Tyrrhenian Sea (Pontinian Islands, Western Mediterranean). Journal of Sedimentary Research 82 (7), 451–463. https://doi.org/10.2110/jsr.2012.42.
Mateu-Vicens, G., Khokhlova, A., Sebastián-Pastor, T., 2014. Epiphytic foraminifera indices as bioindicators in Mediterranean seagrass meadows. Journal of Foraminiferal Research 44 (3), 325–339. https://doi.org/10.2113/gsjfr.44.3.325.
Mattis, A., 1977. Non marine Triasic sedimentation, central High Atlas Montains. Morocco. Journal of Sedimentary Research 47 (1), 107–119. https://doi.org/10.1306/212F7108-2B24-11D7-8648000102C1865D.
Mebrouk, F., Tabuce, R., Cappetta, H., Feist, M., 2009. Charophytes du Crétacé/Paléocène du Moyen-Atlas (Maroc): systématique et implications biochronologiques. Revue de Micropaleontologie 52 (2), 131–139 (in French with English Abstract). https://doi.org/10.1016/j.revmic.2007.08.003.
Mhyaoui, H., Manar, H., Remmal, T., Boujamadoui, M., El Kamel F., Amar, M., Mansouri M., El Amrani El Hassani, I., 2017. Deep quaternary volcanic structures in the central Middle Atlas (Morocco): contributions of aeromagnetic mapping. Bulletin De L'Institut Scientifique, Rabat, Section Sciences De La Terre 38, 111–125.
Michard, A., Frizon de Lamote, D., Saddiqi, O., Chalouan, A., 2008. An outline of the Geology of Morocco. In: Michard, A., Saddiqi, O., Chalouan, A., Frizon de Lamote, D. (Eds.), Continental Evolution: The Geology of Morocco. Structure, Stratigraphy, and Tectonics of the Africa-Atlantic-Mediterranean Triple Jonction. Springer, Berlin, Heidelberg, pp. 1–31. https://doi.org/10.1007/978-3-540-77076-3_1.
Michel, J., Vicens, G.M., Westphal, H., 2011. Modern heterozoan carbonates from a eutrophic tropical shelf (Mauritania). Journal of Sedimentary Research 81 (9), 641–655. https://doi.org/10.2110/jsr.2011.53.
Michel, J., Laugié, M., Pohl, A., Lanteaume, C., Masse, J.-P., Donnadieu, Y., Borgomano, J., 2019. Marine carbonate factories: a global model of carbonate platform distribution. International Journal of Earth Sciences 108, 1773–1792. https://doi.org/10.1007/s00531-019-01742-6.
Miclăuș, C., Tent-Manclús, J.E., Tosquella, J., Martín-Martín, M., Serrano, F., 2025. Eocene stratigraphic sequences in the Prebetic of Alicante (SE Spain) and their correlation with global sea-level and climatic curves. Journal of Marine Science and Engineering 13, 1031. https://doi.org/10.3390/jmse13061031.
Milliman, J.D., 1974. Marine Carbonates. Springer-Verlag, Berlin, Heidelberg, New York, p. 375.
Mohammed, A.A., Anan, T.I., Gheith, A.M., 2022. Mode of Formation of the Coastal Sabkha Sediments in the Coastal Plain of Al-Dafna Plateau. Scientific Journal for the Faculty of Science-Sirte University 2 (2), 33–37.
Moissette, P., 2000. Changes in bryozoan assemblages and bathymetric variations. Examples from the Messinian of Northwest Algeria. Palaeogeography, Palaeoclimatology, Palaeoecology 155 (3–4), 305–326. https://doi.org/10.1016/S0031-0182(99)00124-8.
Moissette, P., 2012. Seagrass-associated bryozoan communities from the late Pliocene of the Island of Rhodes (Greece). In: Ernst, A., Schäfer, P., Scholz, J. (Eds.), Bryozoan Studies 2010, Lecture Notes in Earth System Sciences, 143. Springer, Berlin, Heidelberg, pp. 187–201. https://doi.org/10.1007/978-3-642-16411-8_13.
Murray, J.W., 2006. Ecology and Applications of Benthic Foraminifera. Cambridge university press, p. 426. https://doi.org/10.1017/CBO9780511535529.
Nebelsick, J.H., Rasser, M.W., Bassi, D., 2005. Facies dynamics in Eocene to Oligocene circumalpine carbonates. Facies 51 (1), 197–217. https://doi.org/10.1007/s10347-005-0069-2.
Okada, H., Bukry, D., 1980. Supplementary modification and introduction of code numbers to the low-latitude coccolith biostratigraphic zonation (Bukry, 1973; 1975). Marine Micropaleontology 5, 321–325. https://doi.org/10.1016/0377-8398(80)90016-X.
Parras, A., Casadío, S., 2002. Oyster concentrations from the San Julián Formation, Paleogene of Patagonia, Argentina: Taphonomic analysis and paleoenvironmental

implications. In: De Renzi, M., Pardo Alonso, M.V., Belinchón, M., Peñalver, E., Montoya, P., Márquez-Aliaga, A. (Eds.), Currents Topics on Taphonomy and Fossilization: 3. Taphonomy of the shell concentrations. Oficina de Publicaciones, Ajuntament de Valencia, Valencia, pp. 207–213.
Parras, A., Casadío, S., 2005. Taphonomy and sequence stratigraphic significance of oyster-dominated concentrations from the San Julián formation, Oligocene of Patagonia, Argentina. Palaeogeography, Palaeoclimatology, Palaeoecology 217, 47–66. https://doi.org/10.1016/j.palaeo.2004.11.015.
Pickering, K.T., Cantalejo, B., 2015. Deep-marine environments of the middle Eocene upper Hecho group, Spanish Pyrenees: introduction. Earth-Science Reviews 144, 1–9. https://doi.org/10.1016/j.earscirev.2015.02.001.
Pomar, L., 2001. Types of carbonate platforms: a genetic approach. Basin Research 13 (3), 313–334. https://doi.org/10.1046/j.0950-091x.2001.00152.x.
Pomar, L., Baceta, J.I., Hallock, P., Mateu-Vicens, G., Basso, D., 2017. Reef building and carbonate production modes in the west-central Tethys during the Cenozoic. Marine and Petroleum Geology 83, 261–304. https://doi.org/10.1016/j.marpetgeo.2017.03.015.
Powell, A.J., 1992. Dinoflagellate cysts of the Tertiary System. In: Powell, A.J. (Ed.), A Stratigraphic Index of Dinoflagellate Cysts. Chapman and Hall, London,U.K., pp. 155–251
Powell, J.H., Moh'd, B.K., 2011. Evolution of cretaceous to Eocene alluvial and carbonate platform sequences in central and South Jordan. Geoarabia 16 (4), 29–82. https://doi.org/10.2113/geoarabia160429.
Rauscher, R., Doubinger, J., 1982. Les dinokystes du Maestrichtien phosphaté du Maroc. Sciences Géologiques 35 (3), 97–116 (in French). https://doi.org/10.3406/sgeol.1982.1614.
Reich, S., Di Martino, E., Todd, J.A., Wesselingh, F.P., Renema, W., 2015. Indirect paleo-seagrass indicators (IPSIs): a review. Earth-Science Reviews 143, 161–186. https://doi.org/10.1016/j.earscirev.2015.01.009.
Remacha, E., Fernández, L.P., Maestro, E., Oms, O., Estrada Aliberas, M.R., Teixell Cácharo, A., 1998. The Upper Hecho Group turbidites and their vertical evolution to deltas (Eocene, South-central Pyrenees). In: Excursion Guidebook of the 15th IAS International Congress of Sedimentology Alicante 1-25.
Reymond, C.E., Mateu-Vicens, G., Westphal, H., 2014. Foraminiferal assemblages from a transitional tropical upwelling zone in the Golfe d'Arguin, Mauritania. Estuarine, Coastal and Shelf Science 148, 70–84. https://doi.org/10.1016/j.ecss.2014.05.034.
Riding, J.B., 2021. A guide to preparation protocols in palynology. Palynology 45 (Suppl. 1), 1–110. https://doi.org/10.1080/01916122.2021.1878305.
Robbilard, D., 1978. Etude stratigraphique et structurale du Moyen-Atlas septentrional (région de Taza) - Maroc (Ph.D. thesis). Universite des Sciences et Techniques de Lille, Lille, pp. 178 (in French). https://pepite-depot.univ-lille.fr/LIBRE/Th_Num/1978/50376-1978-7.pdf.
Robbilard, D., 1979. Tectonique synsédimentaire du Moyen-Atlas septentrional au Sud de Taza (Maroc). Bulletin de la Société Géologique de France 21 (4), 441–447 (in French). https://doi.org/10.2113/gssgfbull.S7-XXI.4.441.
Roigé, M., Gómez-Gras, D., Remacha, E., Daza, R., Boya, S., 2016. Tectonic control on sediment sources in the Jaca basin (Middle and Upper Eocene of the South-Central Pyrenees). Comptes Rendus Geoscience 348 (3–4), 236–245. https://doi.org/10.1016/j.crte.2015.10.005.
Roozpeykar, A., Moghaddam, I.M., 2016. Sequence biostratigraphy and paleoenvironmental reconstruction of the Oligocene-early Miocene deposits of the Zagros Basin (Dehdasht area, South West Iran). Arabian Journal of Geosciences 9, 77. https://doi.org/10.1007/s12517-015-2064-4.
Rouvier, H., 1985. Géologie de l'Extrême Nord Tunisien: tectonique et paléogéographie superposées à l'extrémité orientale de la chaîne nord-Maghrébine, 29. Edition du Service géologique de Tunisie. Annales des mines et de la géologie, p. 427 (in French).
Sánchez-Román, M., Gibert, L., Martín-Martín, J.D., van Zuilen, K., Pineda-González, V., Vroon, P., Bruggmann, S., 2025. Sabkha and salina dolomite preserves the biogeochemical conditions of its depositional paleoenvironment. Geochimica et Cosmochimica Acta 356, 66–82. https://doi.org/10.1016/j.gca.2023.06.031.
Sarkar, S., 2019. Alveolina-dominated assemblages in the early Eocene carbonates of Jaintia Hills, NE India: biostratigraphic and palaeoenvironmental implications. Comptes Rendus Palevol 18 (8), 949–966. https://doi.org/10.1016/j.crpv.2019.10.006.
Scheibner, C., Speijer, R.P., 2008. Late Paleocene–early Eocene Tethyan carbonate platform evolution - a response to long- and short-term paleoclimatic change. Earth-Science Reviews 90 (3–4), 71–102. https://doi.org/10.1016/j.earscirev.2008.07.002.
Schlager, W., 2003. Benthic carbonate factories of the Phanerozoic. International Journal of Earth Sciences 92, 445–464. https://doi.org/10.1007/s00531-003-0327-x.
Segonzac, G., Peybernès, B., Rahhali, I., 1986. Les algues du 'Calcaire rosé de Timahdite' (Eocène inférieur) dans le Moyen-Atlas (Maroc): description d'*Halimeda nana* Pia, 1932, dans sa localité-type et son paléoenvironnement. Journal of African Earth Sciences (1983) 5 (5), 501–507 (in French with English Abstract). https://doi.org/10.1016/0899-5362(86)90059-X.
Shili, A., Trabelsi, E.B., Ben Maïz, N., 2002. Benthic macrophyte communities in the Ghar El Melh lagoon (North Tunisia). Journal of Coastal Conservation 8, 135–140. https://doi.org/10.1652/1400-0350(2002)008[0135:BMCITG]2.0.CO;2.
Slimani, H., Louwye, S., Abdelkabir, T., 2010. Dinoflagellate cysts from the Cretaceous–Paleogene boundary at Ouled Haddou, southeastern Rif, Morocco: biostratigraphy, paleoenvironments and paleobiogeography. Palynology 34 (1), 90–124.
Slimani, H., Guédé, K.É., Williams, G.L., Asebriy, L., Ahmamou, M., 2016. Campanian to Eocene dinoflagellate cyst biostratigraphy from the Tahar and Sekada sections at Arba Ayacha, western External Rif, Morocco. Review of Palaeobotany and Palynology 228, 26–46. https://doi.org/10.1016/j.revpalbo.2016.01.003.
Slimani, H., M'Hamdi, A., Uchman, A., Gasiński, M.A., Guédé, K.E., Mahboub, I., 2021. Dinoflagellate cyst biostratigraphy of Upper Cretaceous turbiditic deposits from a part of the Bąkowiec section in the Skole Nappe (Outer Carpathians, southern Poland). Cretaceous Research 123, 104780. https://doi.org/10.1016/j.cretres.2021.104780.
Talmat, S., Martín-Martín, M., Benyoucef, M., Ferré, B., Belhai, D., 2025. The Koudiat El Madene unit (Kabylian "Dorsal", Algeria) and its correlation with similar units belonging to the Rif-Betic Arc (Morocco and Spain). Journal of African Earth Sciences 223, 105515. https://doi.org/10.1016/j. jafrearsci.2024.105515.
Termier, H., 1936. Etude géologique sur le Maroc central et la Moyen Atlas septentrional. Notes et Mémoires du Service des Mines et de la Carte Géologique du Maroc 33, 1566 (in French).
Tomassetti, L., Benedetti, A., Brandano, M., 2016. Middle Eocene seagrass facies from Apennine carbonate platforms (Italy). Sedimentary Geology 335, 136–149. https://doi.org/10.1016/j.sedgeo.2016.02.002.
Toscano, A.G., Lazo, D.G., Luci, L., 2018. Taphonomy and paleoecology of lower cretaceous oyster mass occurrences fromWest-Central Argentina and evolutionary paleoecology of gregariousness in oysters. Palaios 33 (6), 237–255. https://doi.org/10.2110/palo.2017.096.
Tosquella, J., Martín-Martín, M., Guerrera, F., Francisco Serrano, F., Tramontana, M., 2022. The Eocene carbonate platform of the central-western Malaguides (Internal Betic Zone, S Spain) and its meaning for the Cenozoic paleogeography of the westernmost Tethys. Palaeogeography, Palaeoclimatology, Palaeoecology 589, 110840. https://doi.org/10.1016/j.palaeo.2022.110840.
Tosquella, J., Martín-Martín, M., Miclăuș, C., Tent-Manclús, J.E., Serrano, F., Martín-Pérez, J.A., 2025. Eocene gravity flows in the internal Prebetic (Betic Cordillera, SE Spain): a vestige of an Ilerdian lost carbonate platform in the south Iberian margin. Geosciences 15 (3), 81. https://doi.org/10.3390/geosciences15030081.
Trappe, J., 1991. Stratigraphy, facies distribution and paleogeography of the marine Paleogene from theWestern High Atlas, Morocco. Neues Jahrbuch für Geologie und Paläontologie (Abhandlungen) 180 (3), 279–321. https://doi.org/10.1127/njgpa/180/1991/279.
Trappe, J., 1992. Microfacies zonation and spatial evolution of a carbonate ramp: marginal Moroccan phosphate sea during the Paleogene. Geologische Rundschau 81, 105–126. https://doi.org/10.1007/BF01764543.
Tribovillard, N., Bout-Roumazeilles, V., Abraham, R., Ventalon, S., Delattre, M., Baudin, F., 2023. The contrasting origins of glauconite in the shallow marine environment highlight this mineral as a marker of paleoenvironmental conditions. Special Issue "Tribute to Jean Dercourt" of Comptes Rendus Géoscience 355 (S2), 213–228. https://doi.org/10.5802/crgeos.170.
Van Houten, F.B., 1980. Latest Jurassic-early Cretaceous regressive facies, Northeast Africa craton. AAPG Bulletin 64 (6), 857–867. https://doi.org/10.1306/2F9193C8-16CE-11D7-8645000102C1865D.
Vitale, S., Amore, O.F., Ciarcia, S., Fedele, L., Grifa, C., Prinzi, E.P., Tavani, S., Tramparulo, F.D.A., 2018. Structural, stratigraphic, and petrological clues for a Cretaceous–Paleogene abortive rift in the southern Adria domain (southern Apennines, Italy). Geological Journal 53 (2), 660–681. https://doi.org/10.1002/gj.2919.
Westphal, H., Halfar, J., Freiwald, A., 2010. Heterozoan carbonates in subtropical to tropical settings in the present and past. International Journal of Earth Sciences (Geol. Rundsch.) 99 (Suppl. 1), 153–169. https://doi.org/10.1007/s00531-010-0563-9.
Wildi, W., 1983. La chaîne tello-rifaine (Algérie-Maroc-Tunisie): structure, stratigraphie et évolution du Trias au Miocène. Revue de Géologie Dynamique et de Géographie Physique 24 (3), 201–297 (in French).
Williams, G.D., Powell, C.M., Cooper, M.A., Cooper, M.A., Williams, G.D., 1989. Geometry and kinematics of inversion tectonics. In: Inversion Tectonics, 44. Geological Society Special Publications, The Geological Society of London, London, UK, pp. 3–15.
Wray, J.L., 1977. Calcareous Algae. Elsevier Publishers, Amsterdam, p. 190.
Zachos, J.C., Pagani, M., Sloan, L.C., Thomas, E., Billups, K., 2001. Trends, rhythms, and aberrations in global climate 65Ma to present. Science 292, 686–693. https://doi.org/10.1126/science.1059412.